OFFICE OF NAVAL RESEARCH
Task Contract N5ori-07806
NR-026-001

TECHNICAL REPORT NO. 64

DECEMBER 1, 1954

FAST NEUTRON INELASTIC SCATTERING*

By

ROBERT MITCHELL KIEHN

LABORATORY FOR NUCLEAR SCIENCE AND ENGINEERING
MASSACHUSETTS INSTITUTE OF TECHNOLOGY
Cambridge, Massachusetts

Technical Report No. 64

December 15, 1953

FAST NEUTRON INELASTIC SCATTERING*

By

Robert Mitchell Kiehn

*This work is identical in text to a thesis of the same title submitted by the author in partial fulfillment of the requirements for the degree of Doctor of Philosophy in Physics at the Massachusetts Institute of Technology, December, 1953.

This report has been distributed in accordance with the Official Distribution List as approved by ONR letter, ONR 422:WEW, Serial 16132, July 23, 1953.

TABLE OF CONTENTS

LIST OF ILLUSTRATIONS

ABSTRACT

The neutron inelastic scattering cross sections of Fe, Al, Cr, Ni, Pb and Bi have been measured with ~20 kev resolution for neutron energies between 0 and 2.7 Mev. The inelastic event was detected with a single crystal NaI(Tl) gamma ray spectrometer by measuring the yield of the mono-energetic gamma rays emitted by the excited nucleus. The magnitudes of the cross sections are in good agreement with the predicted values as calculated from the Hauser-Feshbach theory. The experimental resolution was good enough to pick out resonant structure in the inelastic cross sections.

The experimental method also allowed the determination of the first few excited states of the stable nuclei observed. The energies of these excited states were found to be in good agreement with values obtained by other means. New levels were found in Bi and I.

The total neutron cross sections of C, Cl and P have also been measured in good geometry and with 2 kev resolution for 100 kev $< E_n <$ 1.2 Mev. Many resonances were observed in the latter two nuclei in agreement with the expected high level densities of their respective compound nuclei.

I INTRODUCTION

An experimental technique for examining the neutron inelastic scattering cross-section of the stable elements has been developed. Such reactions are of interest in the interpretation of the interactions of neutrons with nuclei. Inelastic scattering gives information concerning the compound nucleus and its formation and reveals new energy levels and their characteristics in many nuclei.

The experimental problem is complicated by the lack of adequate fast neutron spectrometers, low neutron yields from monoenergetic neutron sources, and, especially at low neutron energies, low values of the inelastic cross-section itself. Threshold detectors, cloud chambers, photographic plates and to some extent recoil counters have been used to measure the yield of inelastically scattered neutrons as compared to the incident or elastically scattered neutrons (see references 1 - 9 for a review of previous measurements). These techniques are satisfactory for high energy neutrons (>3 Mev) but are either inapplicable or of limited usefulness in the interesting range 0 - 3 Mev, which corresponds to the major yield of fission neutrons.

After several discouraging attempts to measure the inelastically scattered neutrons in this energy range, it was decided instead to study the gamma rays emitted by the excited residual nucleus. It is interesting to note that this method led to the discovery of inelastic scattering by Kikuchi and coworkers in 1935. They used coincidence beta-ray counters with interposed absorbers to measure the energy of the Compton electrons ejected from a metal plate by the inelastic gamma rays.

While the present method is similar in principle, the use of high efficiency, high resolution scintillation spectrometers offers many advantages over these earlier techniques. The photo-electric absorption peak in a NaI crystal was used as a measure of the yield of monoenergetic, inelastic gamma rays. The experimental problems encountered were:

1) The procurement of a relatively high yield of mono-energetic neutrons.
2) The construction of an adequate gamma ray detector of high resolution and sensitivity.
3) The development of a technique whereby the

line spectrum of gamma rays coming from neutron inelastic excitation could be observed effectively in the midst of the high gamma ray background always associated with neutron work. In addition, the gamma ray detector and experimental arrangement must be capable of distinguishing between neutrons and gamma rays.

4) Absolute calibration and interpretation.

In the energy region $0 \leq E_n \leq 2.7$ Mev, most nuclei with $A \leq 70$ have levels which are separated by more than 100 kev. For the heavy nuclei, except those which are magic, the level spacing is of the order of 100 kev or less. This situation imposes extreme demands upon the resolution of the gamma ray detector. After some effort, single crystal NaI(Tl) gamma ray spectrometers were constructed which have a resolution of about 5 per cent for 1.2 Mev gamma rays. As a result the nuclei which may be investigated by this technique are those with level spacings of 100 kev or more. Furthermore, if the element in question has several isotopes, differentiation between isotopes is difficult. Cascade gamma processes could be established by coincidence techniques, but no work of this kind was done.

The elements chosen for study were the reactor constructional materials Al, and Fe, and the magic elements Pb and Bi. This choice illustrates the application of the technique both to light and to medium weight nuclei. Ni and Cr were also investigated and disclose the problems to be encountered when elements with many isotopes are used.

After several preliminary experiments a method was evolved for examination of the inelastic neutron cross section for each of the excited levels of the target nucleus in the same detail as in total cross section measurements. Accordingly experiments were conducted using neutron beams of $\leq$ 25 kev resolution for the first few Mev. Many resonances in the yields of the individual gamma rays were observed. These are attributed to resonance formation in the compound nucleus.

II RESULTS, INTERPRETATIONS AND CONCLUSIONS

II-1 General

The inelastic scattering cross sections of neutrons for Fe, Al, Bi, Pb, Ni and Cr for neutron energies between 0 and 2.7 Mev have been investigated by observing the line spectrum of gamma rays emitted by the residual excited nucleus. By using a high resolution NaI(Tl) single-crystal, gamma-ray spectrometer as a detector, and by observing the pulse height spectrum from the counter, the yield of the line spectrum of gamma rays can be measured in the presence of a high background of neutrons and neutron-induced gamma radiation. Using neutron beams of ≈25 kev energy width, the gamma ray yields for these elements were measured in 50 kev energy intervals for $0<E_n \leq 2.7$ Mev. The yield of gamma rays was then assumed to be proportional to the number of inelastic events taking place in the scatterer, and was accordingly calibrated in terms of the inelastic scattering cross section, σ_{in}.

The measurement of the line spectrum of gamma rays insures that only inelastic events are recorded. If two or more levels are neutron excited and each emits gamma

rays in transitions to the ground state, the cross section for each level excited may be determined. If the gamma rays are in cascade, the lower level gamma ray gives the total inelastic cross section immediately, and a subtraction yields the cross section for the production of each individual level. It is therefore necessary to have some preconception, or a preliminary determination of the energy level diagrams of the nuclei under consideration. Using the incident neutron energy, and the gamma ray energy calibration of the scintillation spectrometer as two independent variables, the level structure of stable nuclei may be determined for those excited states capable of being produced by neutron bombardment.

Figure 1 portrays the results of the above methods for the six elements studied. The levels in Bi^{209} have not been observed before. The other levels indicated have been confirmed by other means.[10 - 12] The gamma-ray transitions shown as solid lines are those as observed and studied for their relative yields. The dashed gamma ray transitions were either too weak to be observed effectively, or were not examined in detail as a function of energy (Fe and Cr).

Fig. 1 Energy Level Diagrams. The energies of the excited levels were determined by measuring the energy of the emitted gamma ray with a scintillation spectrometer. Utilization of the incident neutron energy and the yield of the gamma rays as two independent variables enabled the assignment of cascade processes. The gamma ray yields which were studied in detail as a function of incident neutron energy are shown in solid lines. The dashed lines indicate observed gamma rays which were not studied in detail. The energy assignments given to the individual levels are in agreement with other determinations within the given experimental uncertainty.

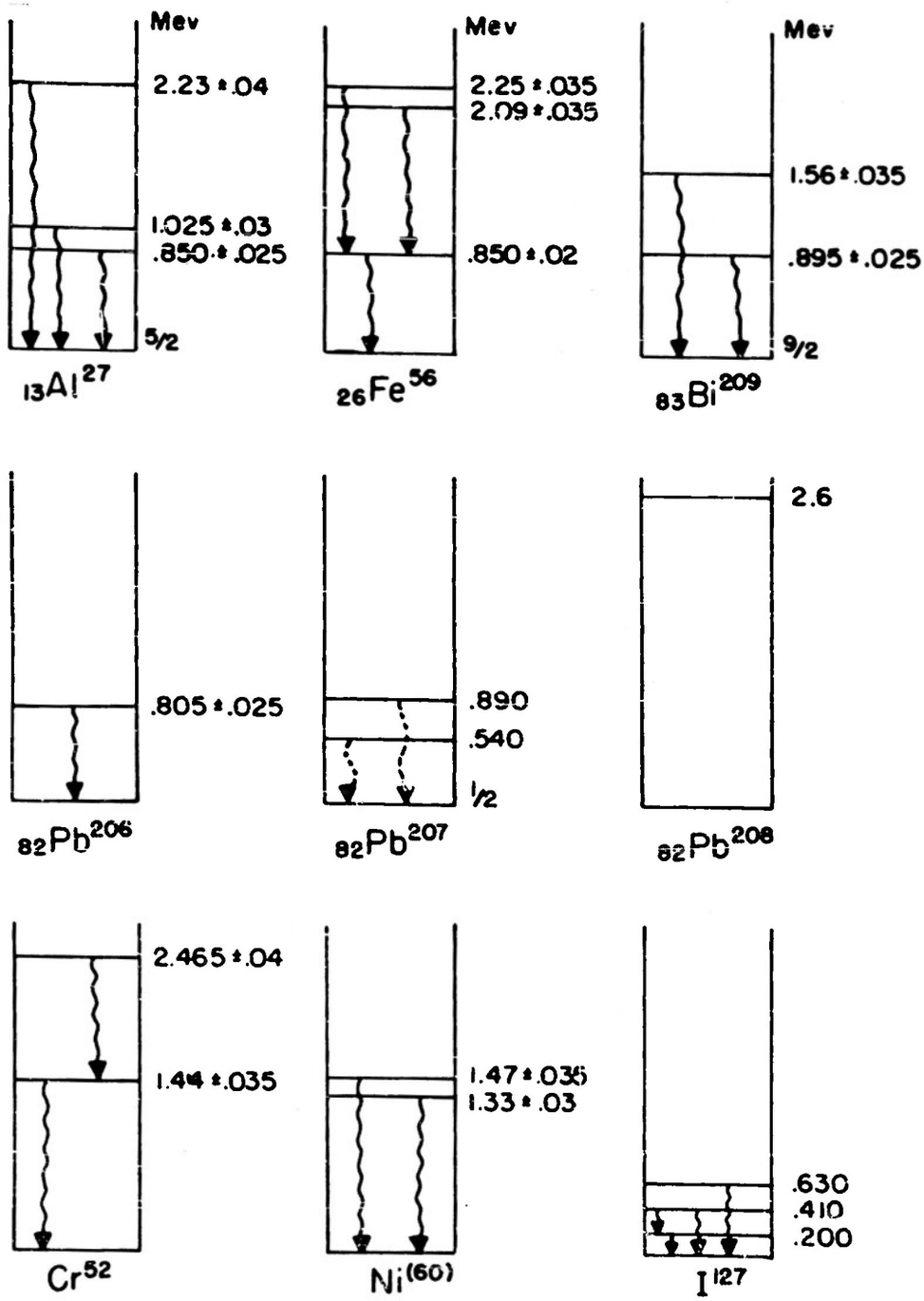
Mev
2.23 ± .04
1.025 ± .03
.850 ± .025
5/2
$_{13}Al^{27}$
Mev
2.25 ± .035
2.09 ± .035
.850 ± .02
$_{26}Fe^{56}$
Mev
1.56 ± .035
.895 ± .025
9/2
$_{83}Bi^{209}$
.805 ± .025
$_{82}Pb^{206}$
.890
.540
1/2
$_{82}Pb^{207}$
2.6
$_{82}Pb^{208}$
2.465 ± .04
1.44 ± .035
Cr^{52}
1.47 ± .035
1.33 ± .03
$Ni^{(60)}$
.630
.410
.200
I^{127}

Figure 1

The absolute values of σ_{in} were obtained by experimentally determining the efficiency of the detector and geometry using a known source of gamma rays distributed throughout the scatterer, and calculating the neutron flux incident upon the scatterer using the Los Alamos data for the neutron yield from the $Li^7(p,n)Be^7$ reaction.[13] This method was applied for the determination of σ_{in} for iron with an estimated uncertainty of 10% at $E_n \simeq 1.3$ Mev; the inelastic cross section for the other elements was then determined relative to iron by applying first order correction terms for self-absorption and detector efficiency, Fig. 2 to 8.

The gamma rays observed were between 800 kev and 2.5 Mev in energy; lower energy gamma transitions were either not investigated in detail or not observed. A high background radiation of 200, 410, and 630 kev gamma rays, produced by $(n,n'\gamma)$ processes in the NaI spectrometer, made determinations of low energy gamma yields difficult. As the gammas investigated fell in the energy interval 800 kev $< E_\gamma <$ 2.5 Mev, no corrections for internal conversion processes were made. The transitions observed were fast (low multipole order); hence, the

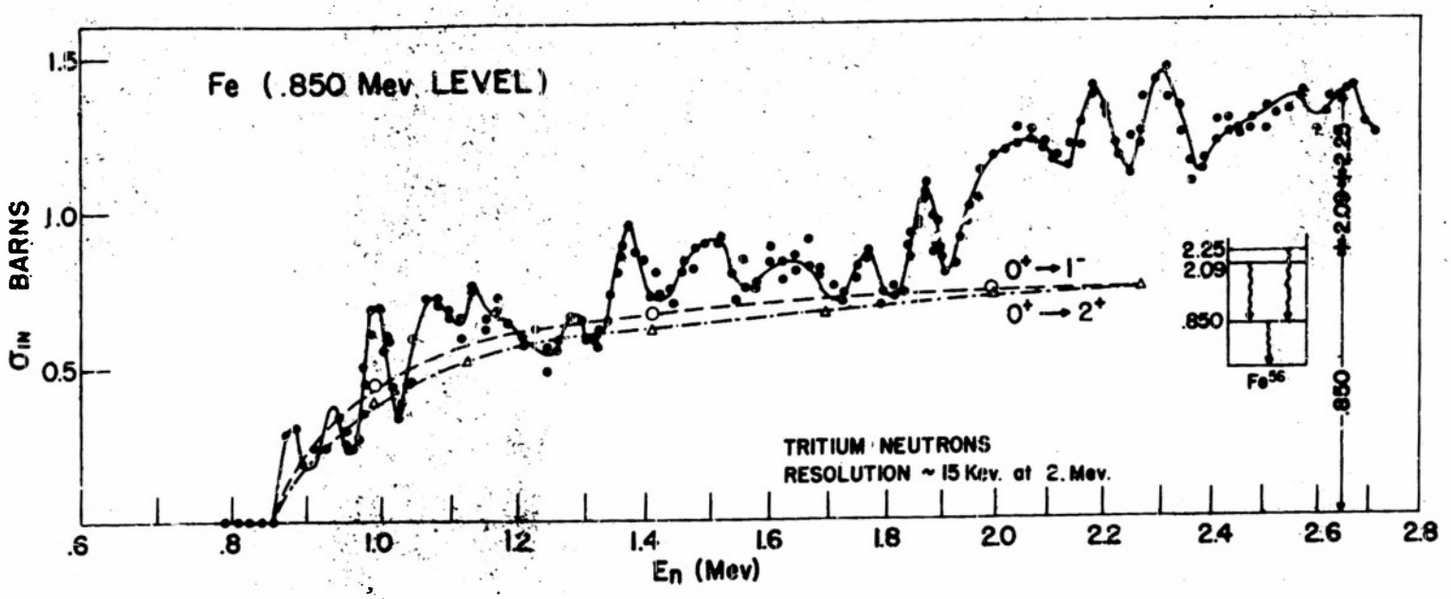

Fig. 2 The Neutron Inelastic Scattering Cross Section of Iron. The data represent the yield of the line spectrum of gamma rays emitted from the excited state of the target nuclei. The ordinate was calibrated by experimentally determining the counter efficiency and by computing the number of neutrons incident upon the scatterer from the measured proton current and target thickness. The neutron energy resolution is ±20 kev. A comparison with the Hauser-Feshbach theory[17] has been made for the single level excitation for the assumed transition $0^+ \rightarrow 1^-$ and $0^+ \rightarrow 2^+$ (the smooth curves). The experimental contributions of the three levels to the total inelastic cross section are given at E_n = 2.64 Mev; note that the 850 kev level contribution falls close to the extrapolated theoretical curve.

Fig. 3 Detail of the Initial Rise of the Reaction $Fe(n,n')^{*}Fe \xrightarrow{\gamma} Fe$. The data represent the yield of the line spectrum of gamma rays emitted by $^{*}Fe^{56}$. The resonance structure in the inelastic scattering cross section, which is clearly defined in the figure, prevents the definite assignment of spin and parity to the excited state by comparison of the slope of the initial rise with the Hauser-Feshbach theory.

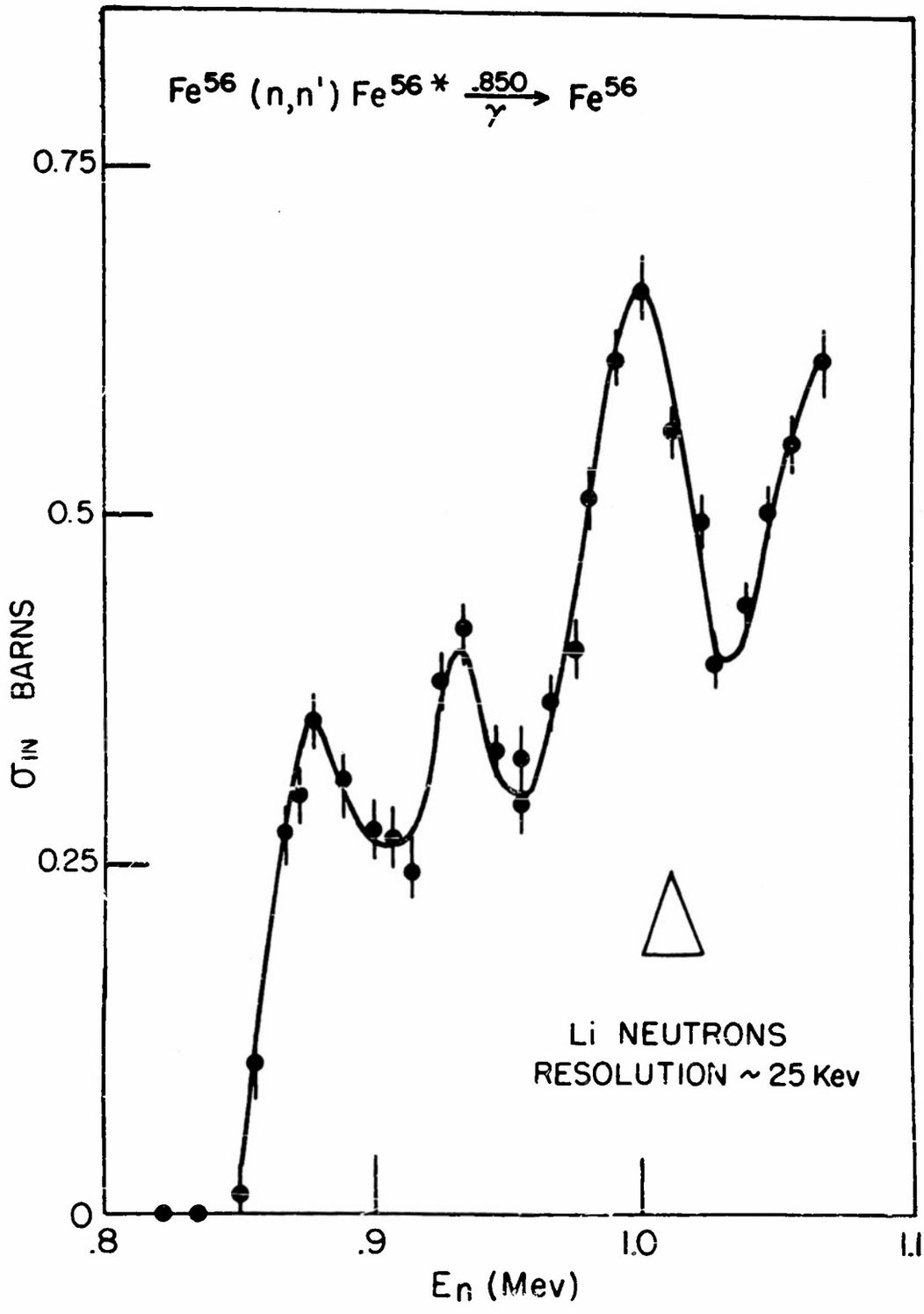
Fe^{56} (n,n') Fe^{56} * $\xrightarrow{.850\ \gamma}$ Fe^{56}
0.75
0.5
0.25
0
σ_{IN} BARNS
.8
.9
1.0
1.1
E_n (Mev)
Li NEUTRONS
RESOLUTION ~ 25 Kev

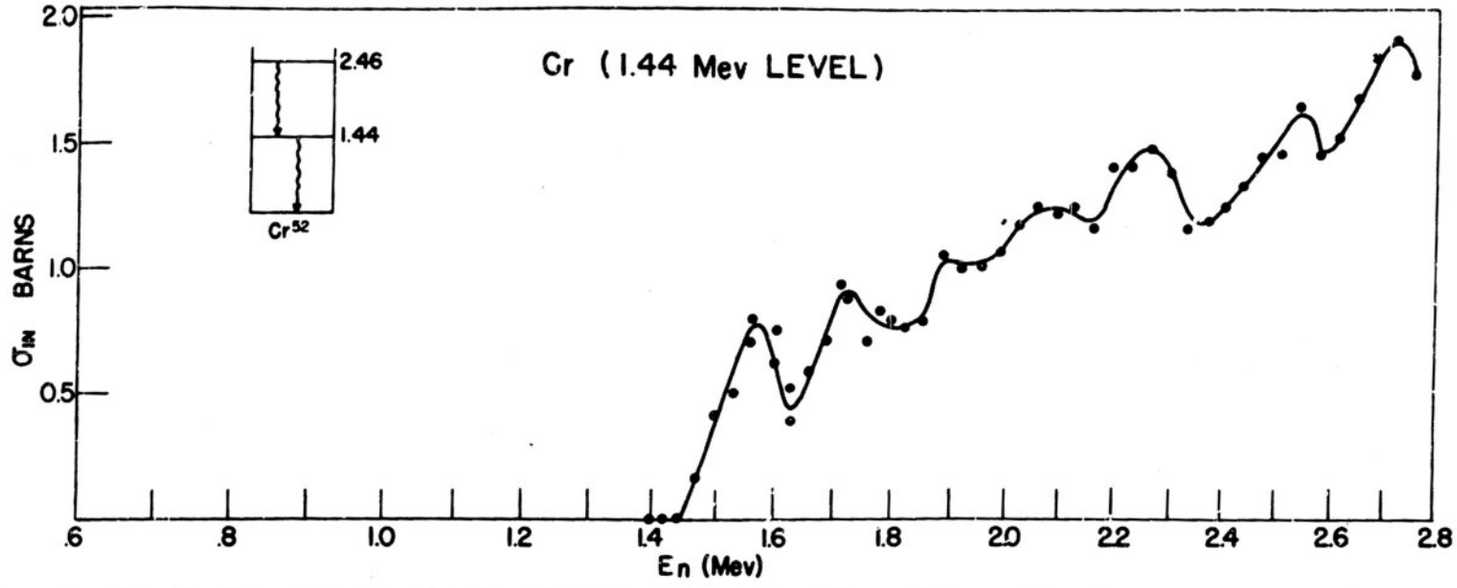

Fig. 5 The Neutron Inelastic Scattering Cross Section of Cr. The data represent the yield of the line spectrum of gamma rays emitted from the excited states of *Cr. The ordinate was calibrated by comparing relative gamma yields with the gamma yield from Fe(n,n'γ)Fe. The neutron energy resolution is ~20 kev.

Fig. 6 The Neutron Inelastic Scattering Cross Section of Ni. The data represent the yield of the line spectrum of gamma rays emitted from the excited states of *Ni. The ordinate was calibrated by comparing relative gamma yields with the gamma yield from Fe(n,n'γ)Fe. The neutron energy resolution is ~ 20 kev. The 1.33 Mev level is in Ni^{60}, while the 1.47 Mev level is probably in Ni^{58}.

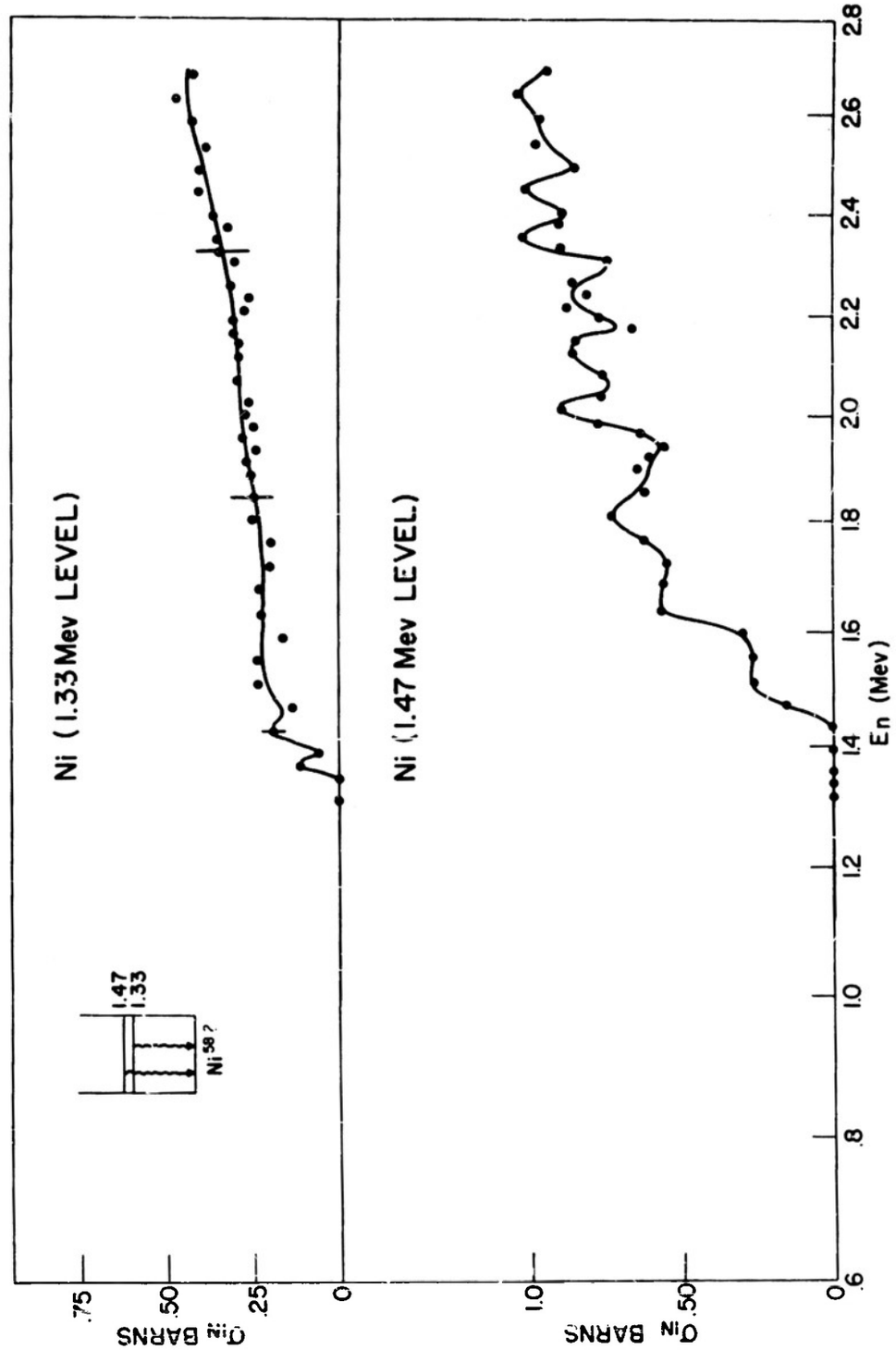
Ni (1.33Mev LEVEL)
Ni (1.47 Mev LEVEL)
1.47
1.33
Ni58 ?
σin BARNS
σin BARNS
En (Mev)
.75
.50
.25
0
1.0
.50
0
.6
.8
1.0
1.2
1.4
1.6
1.8
2.0
2.2
2.4
2.6
2.8

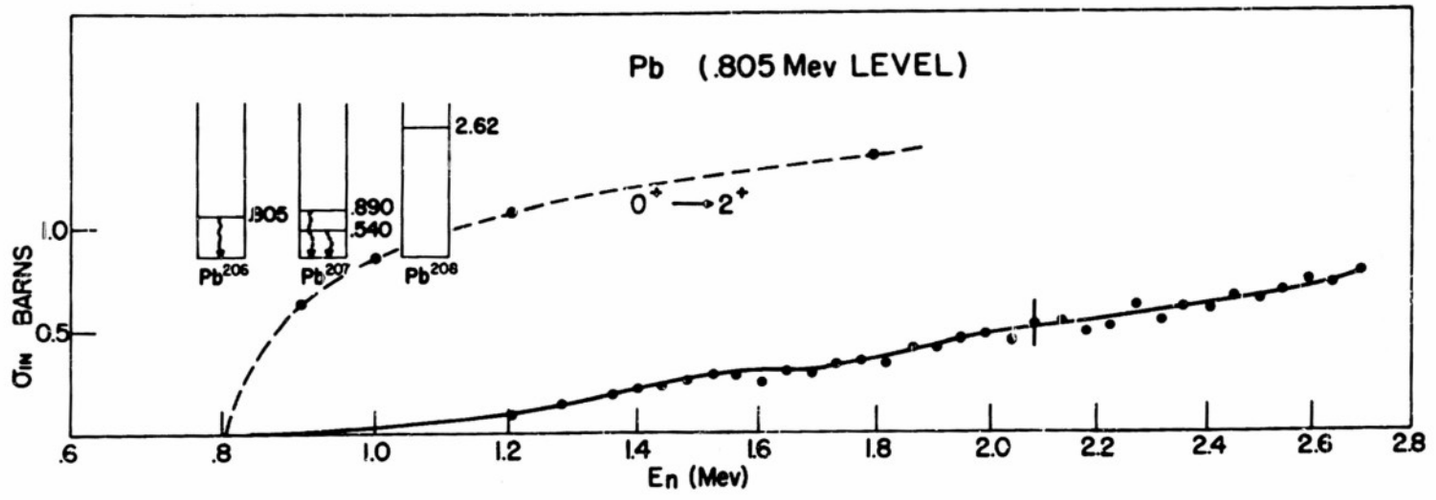

Fig. 7 The Neutron Inelastic Scattering Cross Section of Pb. The data represent the yield of the line spectrum of gamma rays emitted from the excited states of *pb. The ordinate was calibrated by comparing relative gamma yields with the gamma yield from Fe(n,n'γ)Fe. The neutron energy resolution is ~20 kev. A theoretical curve for the assumed transition $0^+ \longrightarrow 2^+$ is also shown. See text for a discussion of the wide disagreement between theory and experiment.

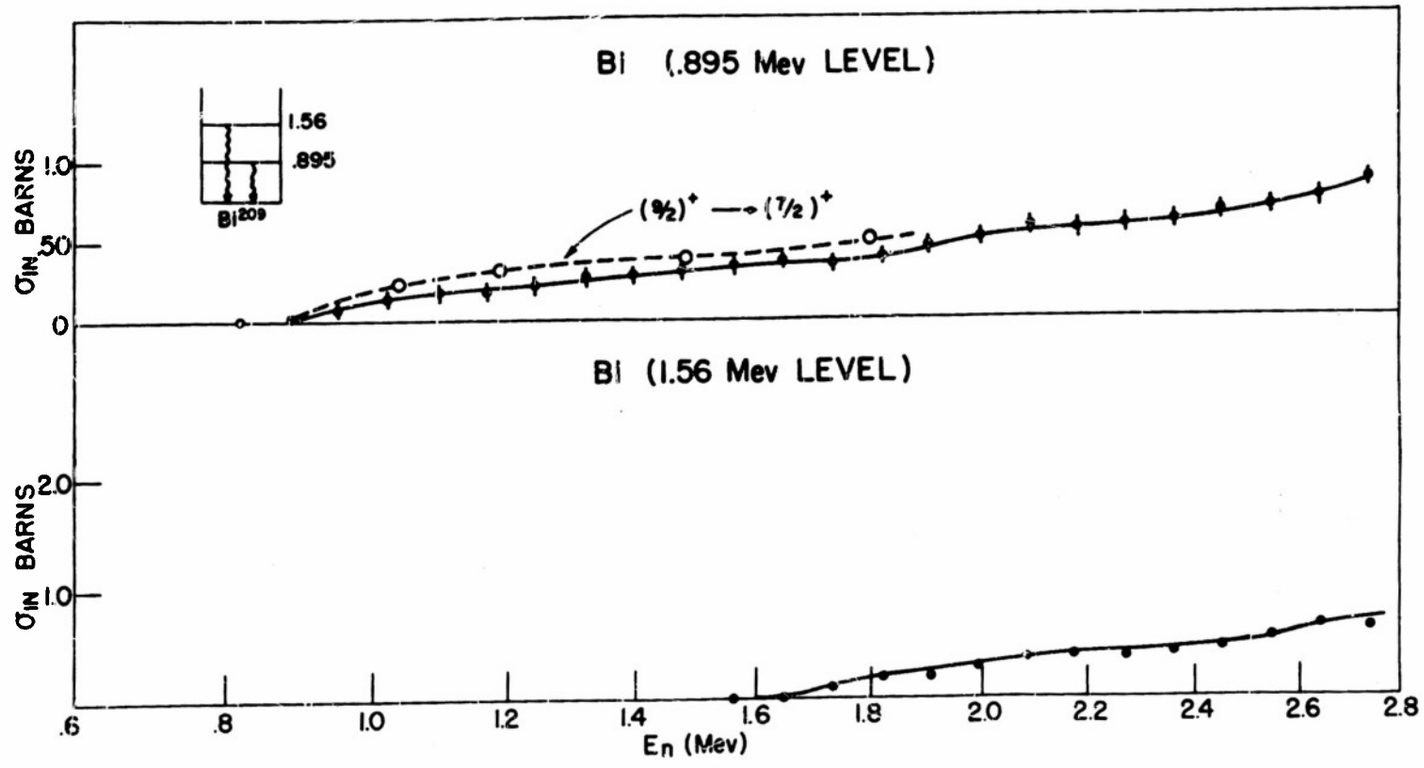

Fig. 8 The Neutron Inelastic Scattering Cross Section of Bi. The data represent the yield of the line spectrum of gamma rays emitted from the excited states of ^{209}Bi. The ordinate was calibrated by comparing relative gamma yields with the gamma yield from Fe(n,n'γ)Fe. The neutron energy resolution is ~20 Kev. A theoretical curve is also shown for the assumed transition $9/2^+ \longrightarrow 7/2^+$.

internal conversion corrections would be small (<5%) even for the heaviest elements.

One obvious fault of the gamma ray technique, in addition to the problems of low energy gamma transitions, finite resolution and complex competing spectra, is the fact that spin 0 to spin 0 transitions are not observed because this gamma transition is completely forbidden.[14]

Many resonances in the inelastic scattering cross sections of the lighter nuclei were observed. These are attributed to resonant formation of the compound nucleus. In most cases, however, the total neutron cross section has not been measured with the same degree of resolution as used in these inelastic cross section experiments. Corrections for the total cross section were based on averaged values.

For one of the major Al resonances both the total and inelastic cross sections were measured simultaneously to show the agreement between resonance structure in both cross sections, Fig. 9.

Experiments in which the spins of the ground state and excited state of the target nucleus, and the spins of the compound levels excited are known would be very significant. Such experiments would yield information

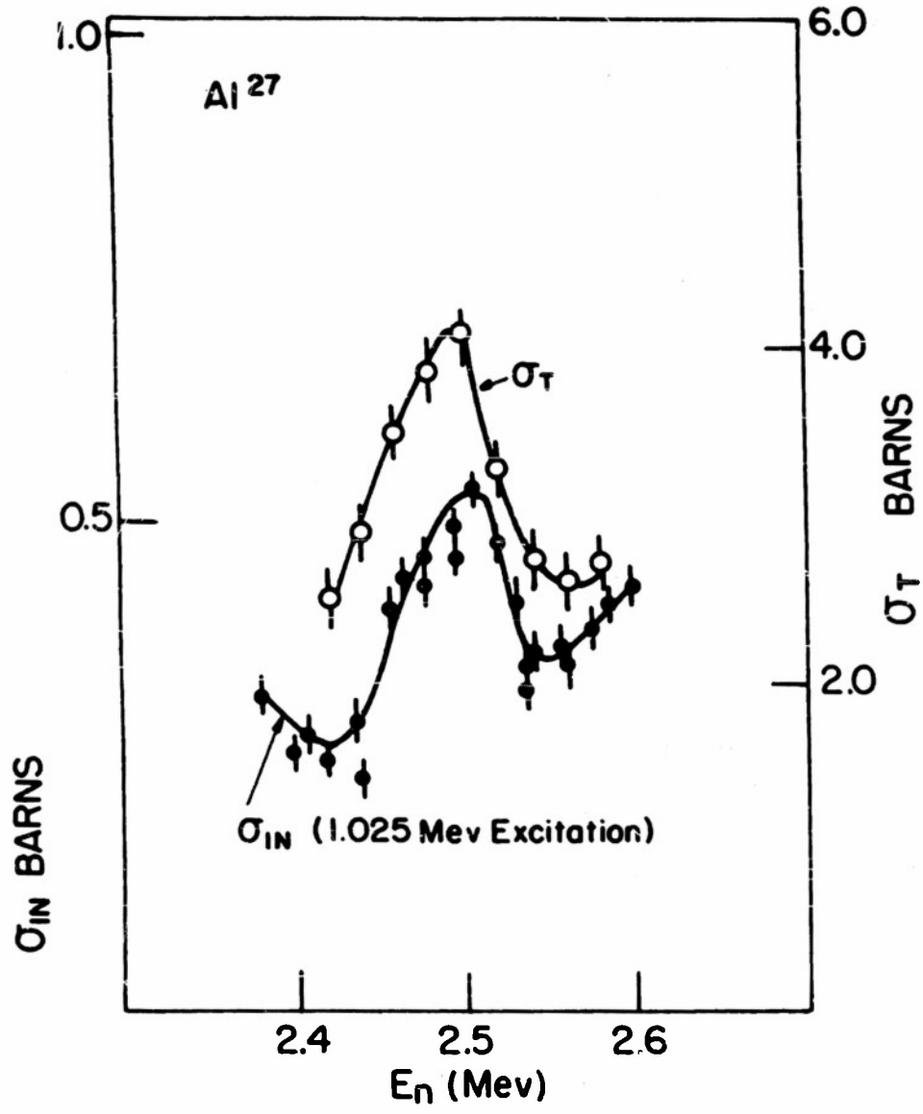

Fig. 9 Comparison of the Resonance Structure in the Total Cross Section and the Inelastic Cross Section of Al. The agreement between the resonance structure of the total neutron cross section and the inelastic neutron cross section indicates that the phenomena are associated with resonance formation of the compound nucleus.

concerning a resonance theory of inelastic scattering. In the elements studied thus far, only the spins of the ground states were known.

It is to be noted that the data obtained for the individual level excitation cross sections immediately give the spectral distribution, x_{in}, of the inelastically scattered neutrons, a quantity of importance in the design of nuclear reactors. For each partial inelastic scattering cross section, the emergent neutron has an energy essentially equal to the incident neutron energy minus the excitation energy of the particular level excited.

II-2 Experimental Results

Fe: The total inelastic cross section of Fe was measured in 30 kev intervals for neutron energies ranging from .80 to 2.7 Mev. The gamma transitions observed were .850 ± .02, 1.26 ± .03 and 1.42 ± .03 Mev. The latter two gamma rays, from levels at 2.09 and 2.25 Mev to the first excited state in Fe^{56} at .850 Mev, were known to be in cascade. Hence, only the yield of the .850 Mev gamma ray was observed in detail. Measurements of the relative contribution of each excited level to the total inelastic

cross section were made for a few neutron energies, Fig. 2. Multiplying the results of Fig. 2 by the fission spectrum and integrating from .4 to 1.4 Mev gives an effective group inelastic scattering cross section of .33 barn, which compares favorably with the Los Alamos values of .313 ± .1 barn.[15]

The spacing of the levels in the inelastic cross-section agree with the data obtained from total cross section measurements.[16]

A theoretical curve for the single level excitation based on the Hauser and Feshbach theory[17] is also shown in Fig. 2; the agreement between theory and experiment is good.

Due to the resonance structure, not too much may be said about the spin of the first excited state, except that it is probably J = 1 or J = 2 (ground state spin = 0).

A more detailed examination of the first three resonances and the initial rise of the inelastic cross section is shown in Fig. 3. The resolution for these data is about 25 - 30 kev, in comparison with about 15 - 20 kev for the data in Fig. 2.

Al: The partial inelastic cross sections of Al resulting in the production of the .850 ± .025, 1.025 ± .03 and the 2.23 ± .04 Mev excited states of Al^{27} were measured for neutron energies from .80 to 2.7 Mev, Fig. 4.

High background prevented the detection of any cascade radiation from the 1.025 Mev to the .850 level (E_γ = .165 Mev), and so it is impossible to determine the individual partial cross-sections if cascade processes are taking place. The sum of the two curves yields the total inelastic neutron cross-section. The different shapes of the two yield curves, (that is, the lack of resonance correlation), indicate that cascade processes are not predominant. Although at first glance it appears that the emission of 850 kev radiation does not begin until the 1.025 Mev radiation is possible energetically, indicating cascades, a closer examination reveals that the .850 Mev level is excited slightly before the 1.025 Mev level. A possible explanation may be that in Al single compound levels are formed at these energies. Perhaps no levels of the compound nucleus have the correct J to allow a large inelastic yield of .850 Mev radiation until $E_\gamma >$ 1.02 Mev. Again, the lack of resonance structure correlation indicates the action of strong selection rules. The ground state of Al^{27} is known to be J = 5/2.

Ni: The total inelastic scattering cross section of Ni has been studied in 50 kev intervals from .80 < E_n < 2.7 Mev, Fig. 6. Radiations to the ground state of 1.33 ± .03 Mev and 1.475 ± 0.35 Mev indicate that the inelastic scattering is due to excitation of levels in Ni^{60} and Ni^{58}, respectively. The lower energy gamma ray is obscured by high Compton background of the 1.47 Mev radiation. The two gamma rays are only partially resolved, Fig. 15. A possible third radiation at 1.025 Mev was observed, but was too weak to examine in detail. Absolute measurements were made relative to Fe.

Pb: The partial inelastic cross section of Pb was examined in 50 kev intervals from .80 < E_n < 2.7 Mev, Fig. 7. Gamma radiation of .805 ± .025 Mev was attributed to the inelastic excitation of the first excited state in Pb^{206}. Radiations of .540 Mev and .890 Mev were also observed and attributed to excitation of Pb^{207}, but were not studied in detail because the yield of these gamma rays was too weak to be separated effectively from the background. The 2.6 Mev level in Pb^{208} was not studied.

The very slow rise of the inelastic cross section indicates a high spin change between the ground state and

the excited state, if the Hauser-Feshbach theory is applicable ($\Delta J > 3$). However for a spin change greater than 4, the first excited state would be metastable. No indication of a metastable state was found; the lifetime of the state was established as less than 10 seconds. The .805 Mev level has approximately the correct energy to be a vibrational level of the nucleus. Accordingly, the shape of the inelastic cross section is expected to be different from that predicted by the Hauser-Feshbach theory. Little evidence of resonant structure indicates that the statistical approximation for the compound nucleus is valid, if the compound nucleus is formed. The disagreement between the theoretical $0^+ \rightarrow 2^+$ transition and the experimental data gives rise to the belief that the compound nucleus is not formed and that the interaction is due to surface excitation of the nucleus. The absolute value of the cross section was determined relative to Fe. An effective group inelastic scattering cross section for fission spectrum neutrons of $.4 \leq E_n \leq 1.4$ Mev of .04 barn was obtained to compare with the Los Alamos value of .168 ± .1 barn, Appendix I. The value so calculated using the data in Fig. 7 does not include the contributions from the excited states in Pb^{207}.

Bi: The partial inelastic scattering cross sections of Bi were examined in ~80 kev intervals from .80 < E_n < 2.7 Mev. Gamma transitions to the ground state gave indications of the first two excited states in Bi^{209} at .895 ± .025 Mev and 1.57 ± .035 Mev, Fig. 8. The ground state of Bi is known to be J = 9/2; a theoretical curve for a J = 7/2 → J 9/2 transition was computed and appears in the figure. The first excited state was assumed to be J = 7/2 on the basis of the shell model.[14]

Again the absolute value of the cross section was determined relative to Fe. An effective group inelastic scattering cross section for fission spectrum neutrons of .4 ≤ E_n ≤ 1.4 Mev of .10 barn was obtained to compare with a Los Alamos value of .168 ± .1 barn, Appendix I.

II-3 Theoretical Interpretations

Several calculations based on the theory of Hauser and Feshbach[17] were attempted in order to compare the theoretical predictions with the experiments. The results

of such calculations, based on the assumption that the level density of the compound nucleus can be treated statistically, should be comparable to an average over the resonance in the experimental cross sections.

The results of the calculations for the excitation of the first excited state in Fe^{56}, indicated in Fig. 2 for $0+ \rightarrow 1-$ and $0+ \rightarrow 2+$ transitions, are in very good agreement with the experimental data. These curves were not normalized, but are based on absolute cross section values as determined both experimentally and theoretically. Similar successes have been observed with the Hauser-Feshbach theory by Margolis.[30] Due to the resonance structure in the inelastic cross section, definite spin-parity assignments cannot be made by comparing the shapes of the experimental and predicted curves for this particular nucleus.

Above 2 Mev the experimental excitation curve for Fe again begins to rise, indicating that more levels are being excited. At a neutron energy of 2.62 Mev, an experimental determination of the relative contributions of each level to the total inelastic cross section was made, Fig. 2. The contribution of the 850 kev level agrees quite well with the extrapolated theoretical curve. All calculations neglected contributions of

neutrons with l or l' greater than 3.

A similar analysis was done for the first excited state in Bi^{209}, Fig. 8. The spin of the excited state was predicted to be 7/2 on the basis of shell theory; the ground state spin is known to be 9/2. Absolute magnitude agreement between the calculated no parity change transition and the experimental results is again good. However, the shape of the yield curve seems to indicate that a higher spin transition is needed to explain the slow initial rise. The slow initial rise of Pb^{206} is even more striking. A spin transition of $0^+ \longrightarrow 2^+$ (i.e., J = 2 for the first excited state following the Goldhaber rule) does not account for low value of σ_{in} above threshold, Fig. 7; a spin change of at least 4, and more likely 5, would be necessary if the Hauser-Feshbach analysis is to be applied. If Pb^{206} was similar to Pb^{204} (with a J = 2 level at 353 kev and a J = 7 level at 1.26 Mev), the slow yield rise of the .805 Mev radiation could be explained by the Hauser-Feshbach theory on the basis of competing neutron emission widths. However, α decay experiments indicate that the first excited level does have a spin J = 2 at .803 Mev, indicating that perhaps the compound

nucleus assumption is not valid for this particular level. Application of the "collective"-model, neutron inelastic scattering theory[23] should be made to Pb^{206} $(n,n'\gamma)Pb^{206}$.

Calculations for Al were not done because the statistical assumption for the compound nucleus is not valid over the energy range investigated. As the spins of the compound states are not known, a resonance theory analysis would also be difficult. However, similar experiments conducted for elements whose ground, excited, and compound state spins are known would yield information suitable for checking with a resonance, inelastic scattering theory. B^{11} is a suitable element for such a study as all pertinent J values are known for those levels excited by neutrons of energy less than 3 Mev. (See Section IV).

III EXPERIMENTAL TECHNIQUES

III-1 Experimental Method

Using the Rockefeller electrostatic generator[18] as a proton accelerator and the $Li^7(p,n)Be^7$ and $T(p,n)He^3$ reactions as a source of mono-energetic neutrons, the energy dependence of the neutron inelastic scattering cross section of several elements was examined by observing the yield of the line spectrum of gamma rays emitted by the de-exciting target nucleus. A single crystal NaI(Tl) spectrometer (shielded from the direct neutron beam and the gamma rays produced in the target by an eight inch cone of Pb) was used to detect the gamma rays. A conical scatterer surrounding the crystal and shielding the spectrometer from gamma rays produced in the walls and floor of the room, partially compensated for the low counting rates expected by increasing the geometrical solid angle subtended by the scatterer, Fig. 10.

In most cases, the scattering sample was of the order of two mean free paths in length for the incident neutrons, which necessitated correcting the incident

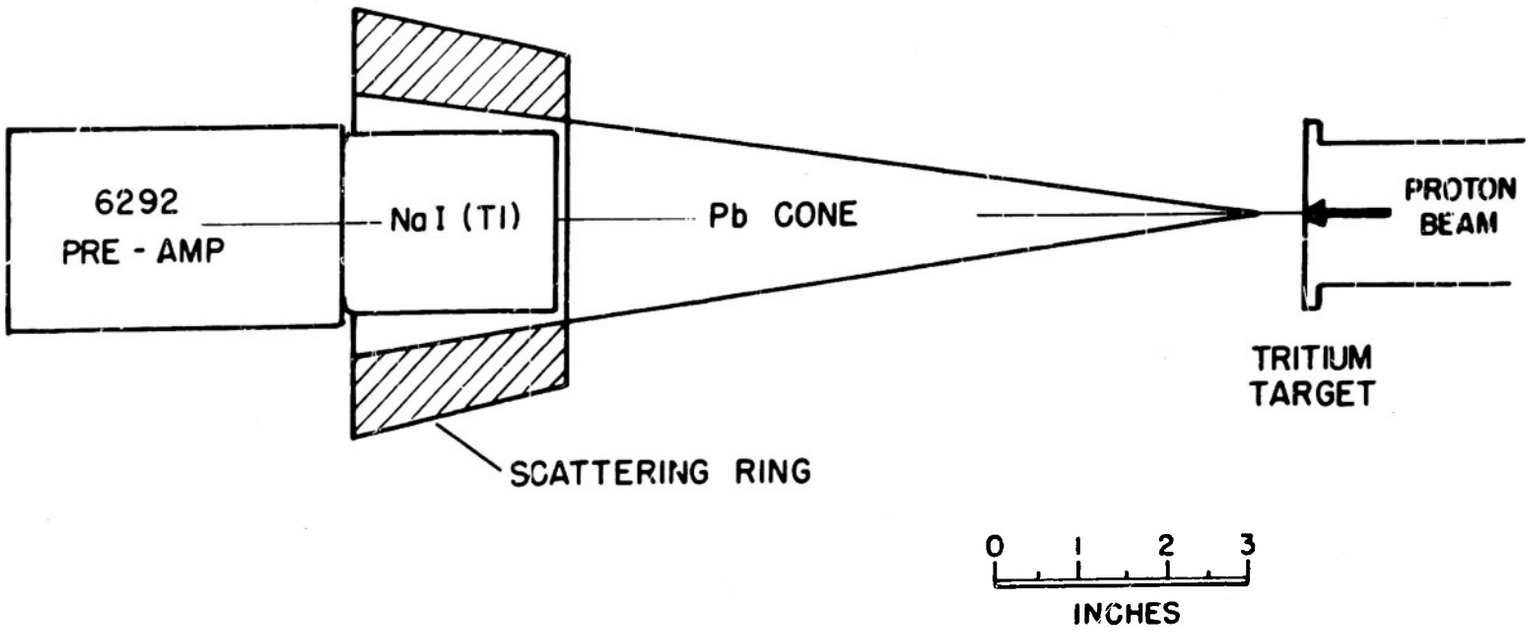

Fig. 10 Experimental Geometry. The single crystal NaI(Tl) spectrometer is mounted inside and coaxial with the conical scatterer and is shielded from the direct neutron beam by the 8" cone of Pb. This "poor" geometry provides good resolution in the energy of neutrons incident upon the scatterer and a large solid angle for the emitted gamma rays. The scatterer also in part shields the crystal from background neutrons and gammas.

flux for beam attenuation. Scattering-in and secondary collision processes were neglected. The beam attenuation factors were based on total cross section averages, Fig. 11.

The sample thickness was of the order of one mean free path for the gamma rays observed, and first order corrections for self absorption in the scatterer were applied to the data.

The neutron beam was monitored by means of enriched BF_3 long counters placed at 110° with respect to the proton beam. Preliminary measurements gave a calibration between the flux incident upon the scatterer and the flux incident upon the neutron monitors, Fig. 4. A pulse height analysis of the gamma ray spectrum produced by the scatterer obtained with the aid of a ten channel, pulse analyzer gave an indication of the number of inelastic neutron events taking place in the scatterer per incident neutron. The gamma ray lines observed were determined to be produced by the inelastic neutron scattering process merely by lowering the energy of the neutrons slightly below the energy of the gamma ray, and checking to see if the yield of line spectrum gamma rays vanished. If the gamma ray line disappeared,

Fig. 11 Neutron Beam Attenuation Factors, and the Ratio of the Yield of Neutrons at 0° to the Yield of Neutrons at 110° for the Reaction $T(p,n)He^3$ vs E_n. Averaged values of the total cross section were used in determining beam attenuation corrections: $\frac{1-e^{-\Sigma_t x}}{\Sigma_t}$. The value for Cr is an educated guess, as no data are available.

The yield ratios were experimentally determined by measuring the neutron flux with BF_3 long counters. The ordinate is a relative value.

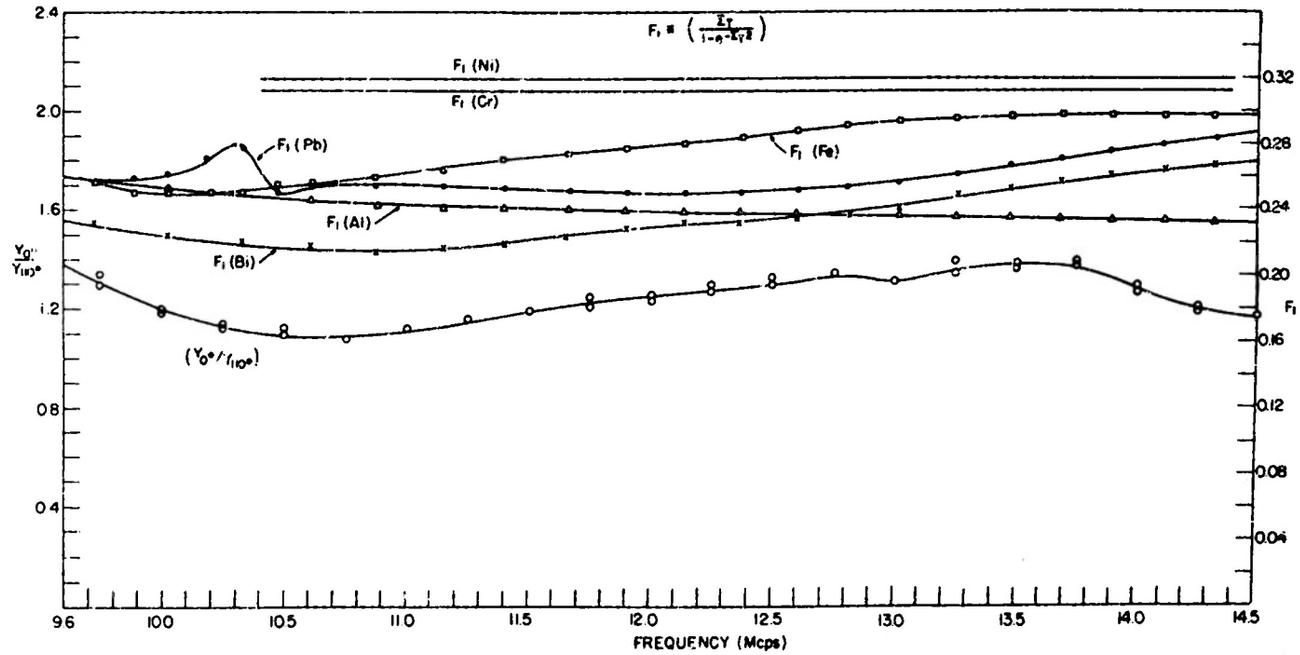
$F_1 = \left(\frac{\Sigma Y}{1-\theta^2\Sigma Y^2}\right)$
F_1 (Ni)
F_1 (Cr)
F_1 (Pb)
F_1 (Fe)
F_1 (Al)
F_1 (Bi)
$(Y_{0°}/Y_{180°})$
$\frac{Y_{0°}}{Y_{180°}}$
F_1
2.4
2.0
1.6
1.2
0.8
0.4
0.32
0.28
0.24
0.20
0.16
0.12
0.08
0.04
9.6
10.0
10.5
11.0
11.5
12.0
12.5
13.0
13.5
14.0
14.5
FREQUENCY (Mcps)

the gamma ray was attributed to an inelastic neutron process. An energy calibration of the crystal spectrometer gave a second check as to the energy of the excited states in the target nucleus so measured. Sample gamma ray spectra appear in Figs. 12 to 18.

The peak value of the resulting line spectrum of gamma rays, obtained by subtracting out a suitable background (which was determined by measuring the pulse height spectrum of capture gamma rays at a neutron energy slightly below the threshold for the inelastic process) was used as a measure of the inelastic neutron cross-section σ_{in}.

If the neutron flux incident upon the scatterer of area A and length Z is represented by φ_0, the number of inelastic events taking place is

$$A\,\varphi_0\,\frac{\Sigma_i}{\Sigma_t}\left(1-e^{-\Sigma_t Z}\right) \qquad (1)$$

and if only one level of the nucleus is excited, the above quantity is equal to the number of gamma rays produced by inelastic neutron scattering.

As some of these gamma rays are self-absorbed by the scatter of thickness T, the number of gamma rays

Fig. 12 Sample Gamma Ray Spectrum for $Fe(n,n'\gamma)Fe$. The single crystal NaI(Tl) spectrometer pulse height analysis gives an indication of the relative yield of the line spectrum of gamma rays superposed upon the continuous background. E_n = 2.6 Mev.

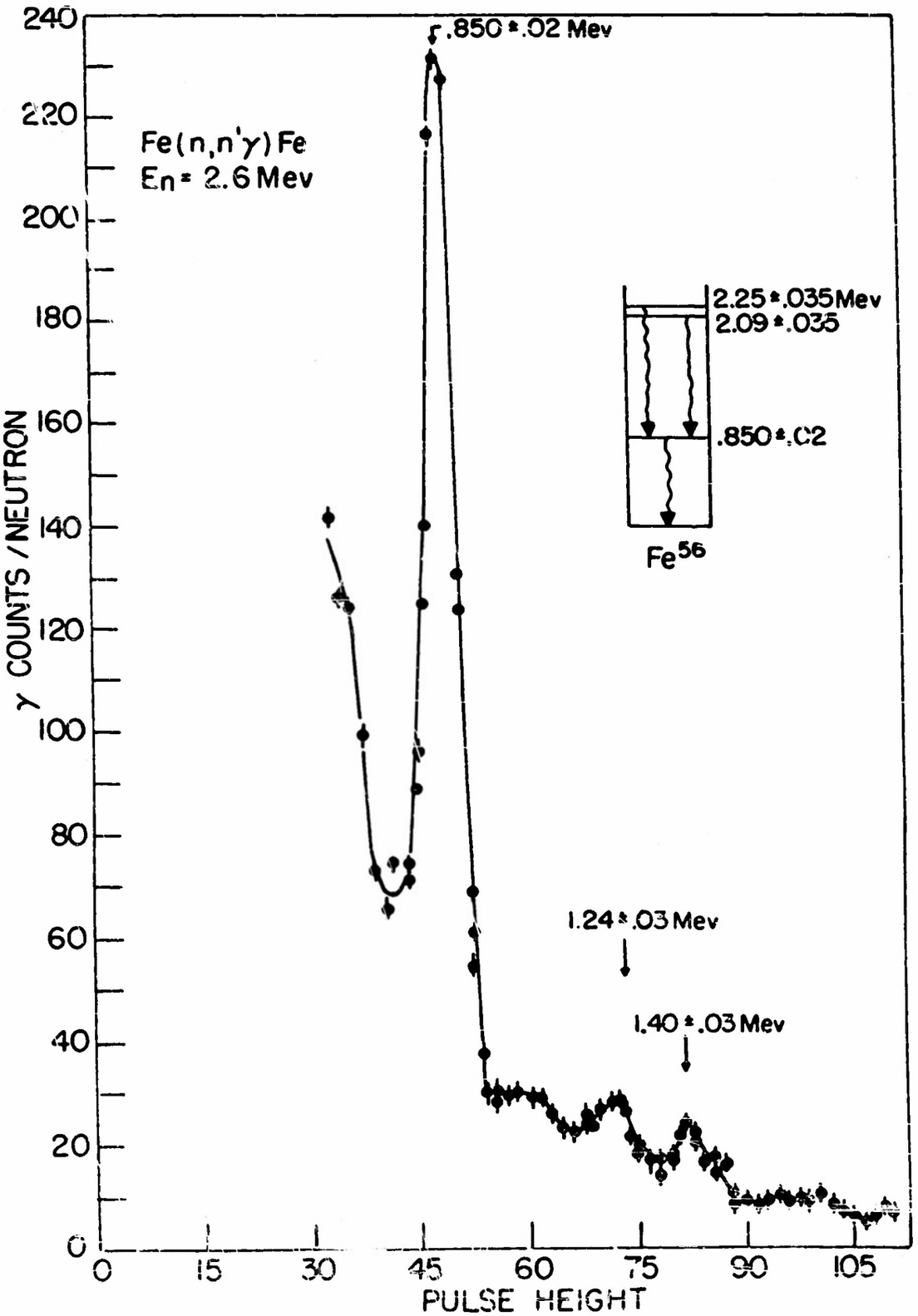
.850 ± .02 Mev
Fe(n,n'γ)Fe
En = 2.6 Mev
2.25 ± .035 Mev
2.09 ± .035
.850 ± .02
Fe56
1.24 ± .03 Mev
1.40 ± .03 Mev
γ COUNTS / NEUTRON
PULSE HEIGHT
0
20
40
60
80
100
120
140
160
180
200
220
240
0
15
30
45
60
75
90
105

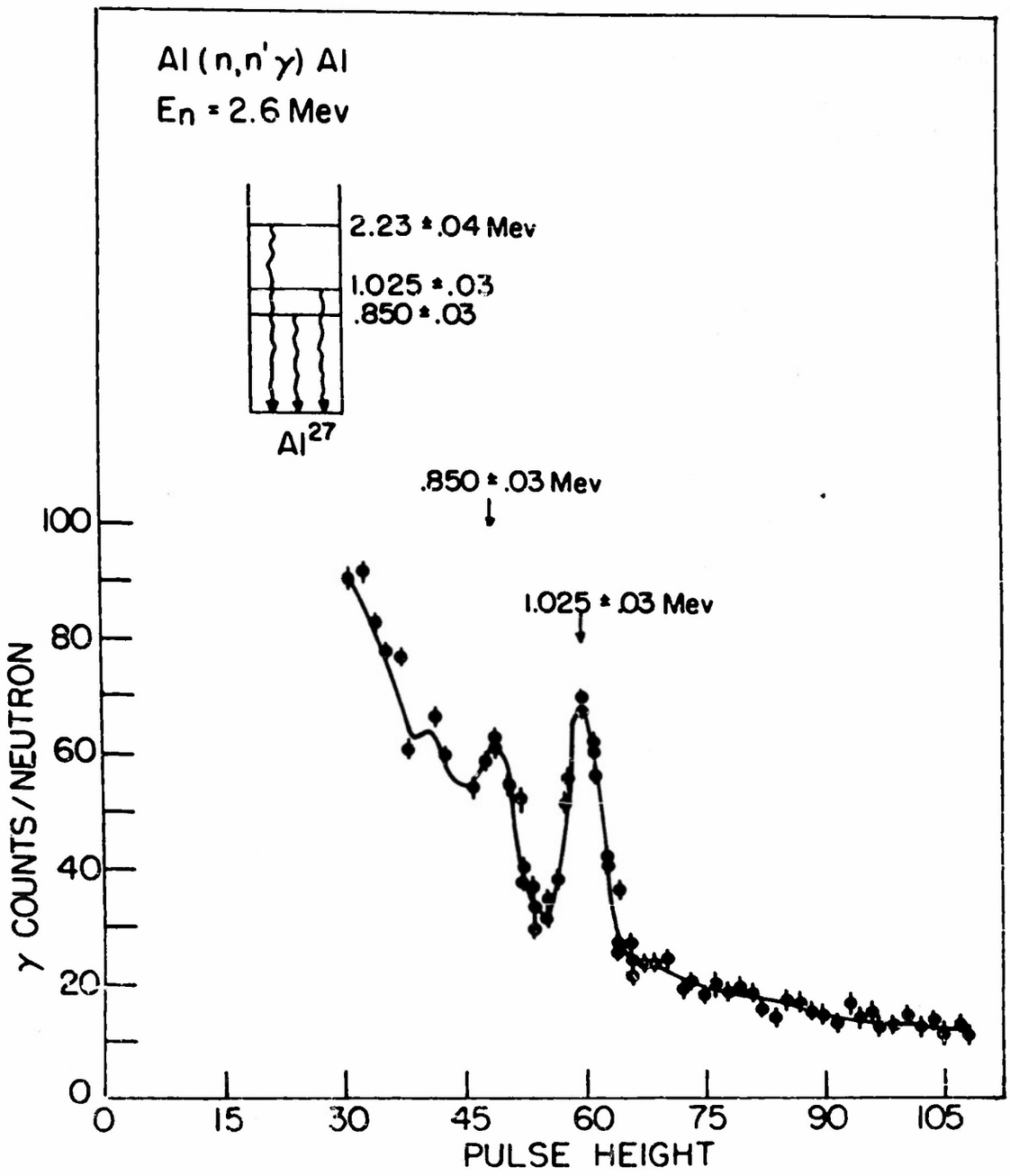

Fig. 13 Sample Gamma Ray Spectrum for Al(n,n'γ)Al. The single crystal NaI(Tl) spectrometer pulse height analysis gives an indication of the relative yield of the line spectrum of gamma rays superposed upon the continuous background. E_n = 2.6 Mev.

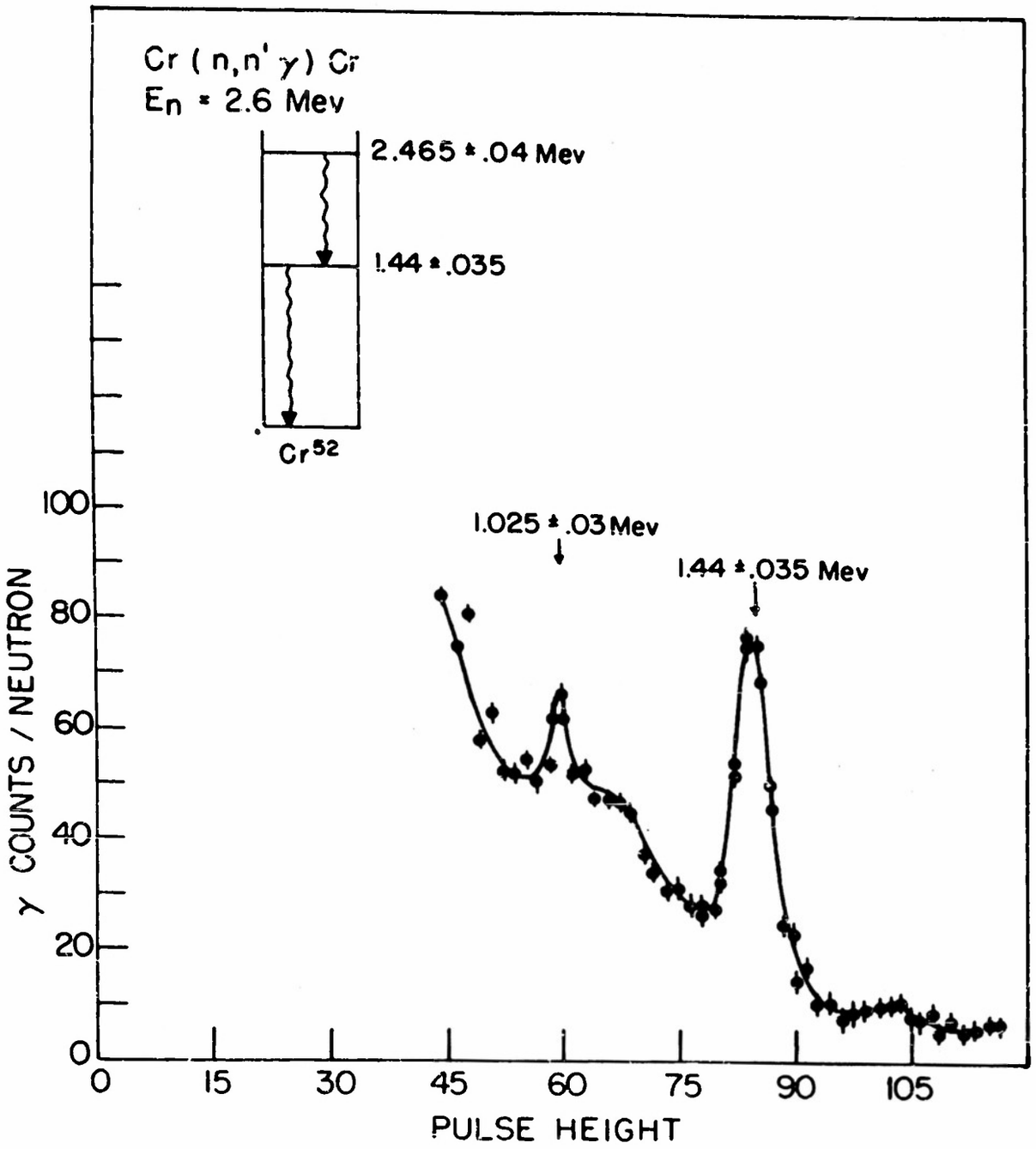

Fig. 14 Sample Gamma Ray Spectrum for Cr(n,n'γ)Cr. The single crystal NaI(Tl) spectrometer pulse height analysis gives an indication of the relative yield of the line spectrum of gamma rays superposed upon the continuous background. E_n = 2.6 Mev.

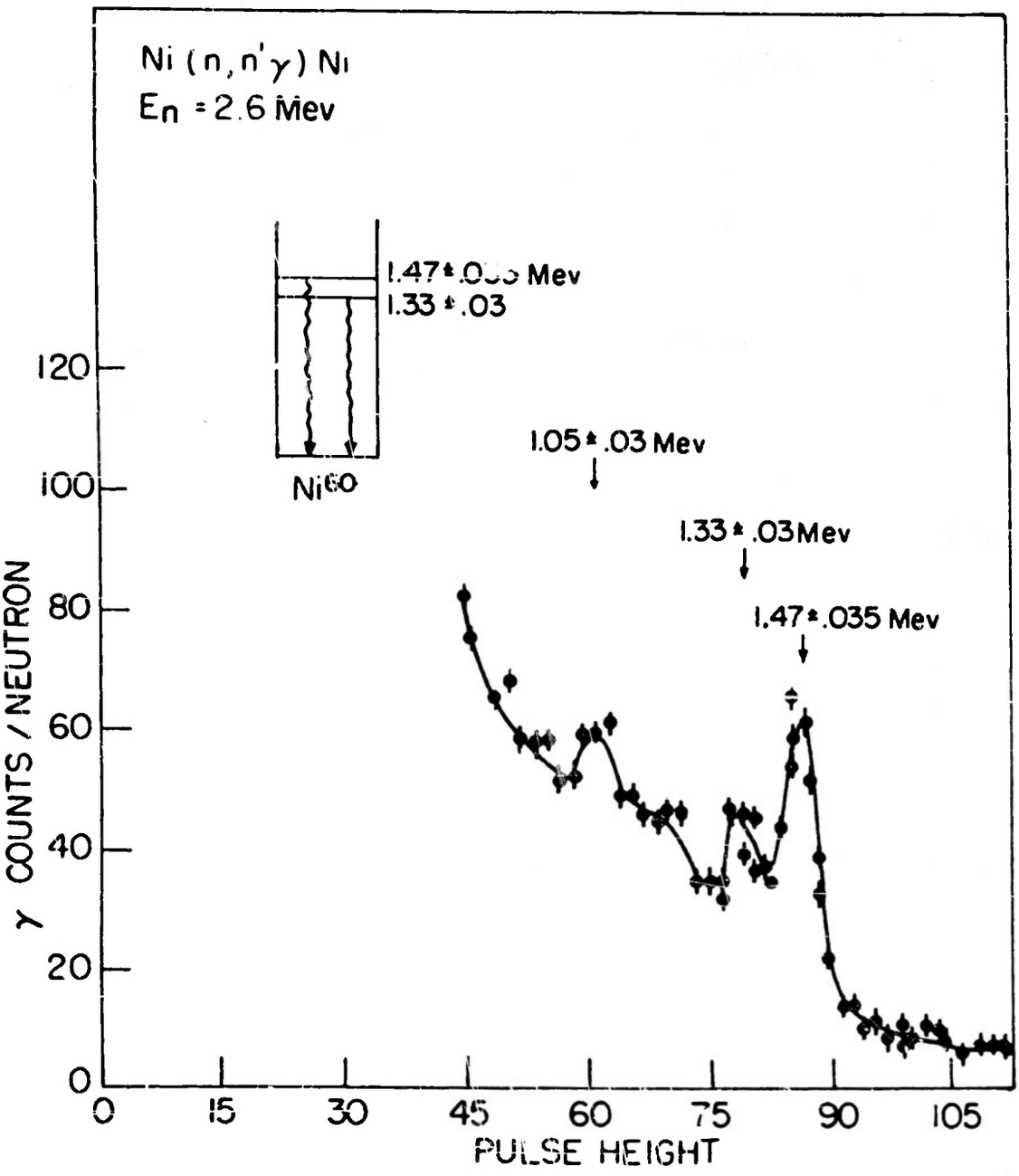

Fig. 15 Sample Gamma Ray Spectrum for Ni(n,n'γ)Ni. The single crystal NaI(Tl) spectrometer pulse height analysis gives an indication of the relative yield of the line spectrum of gamma rays superposed upon the continuous background. E_n - 2.6 Mev.

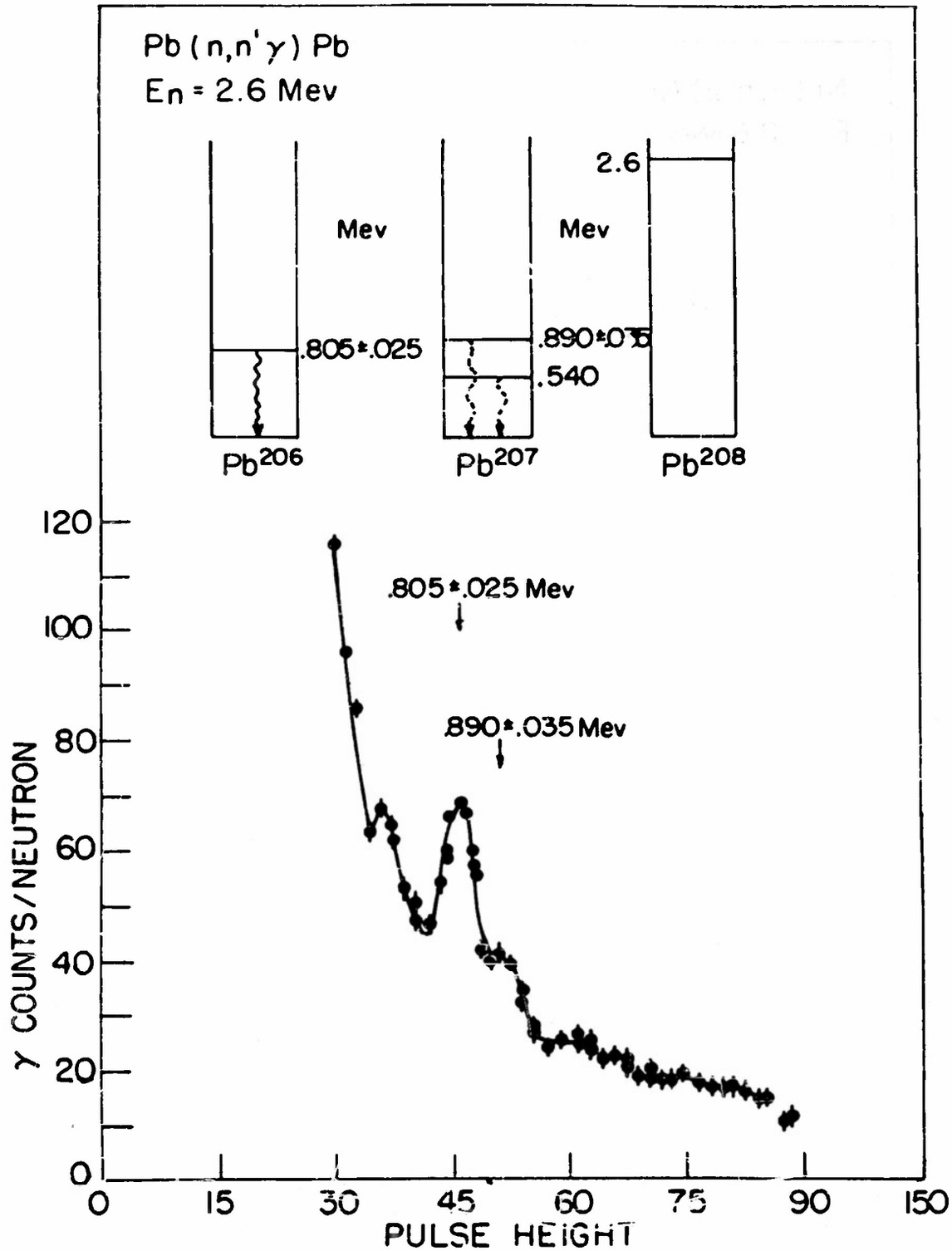

Fig. 16 Sample Gamma Ray Spectrum for Pb(n,n'γ)Pb. The single crystal NaI(Tl) spectrometer pulse height analysis gives an indication of the relative yield of the line spectrum of gamma rays superposed upon the continuous background. E_n = 2.6 Mev.

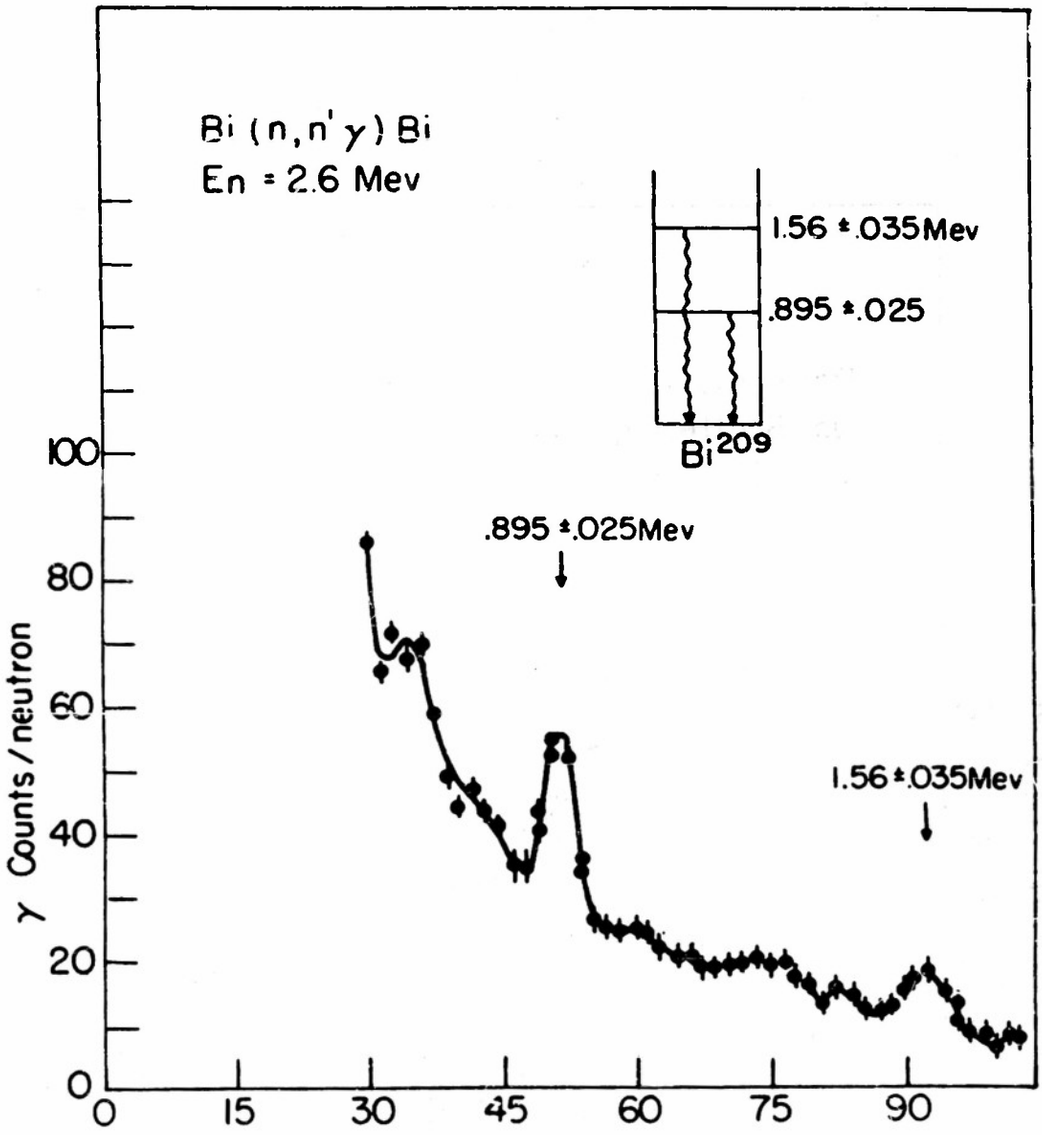

Fig. 17 Sample Gamma Ray Spectrum for Bi(n,n'γ)Bi. The single crystal NaI(Tl) spectrometer pulse height analysis gives an indication of the relative yield of the line spectrum of gamma rays superposed upon the continuous background. E_n = 2.6 Mev.

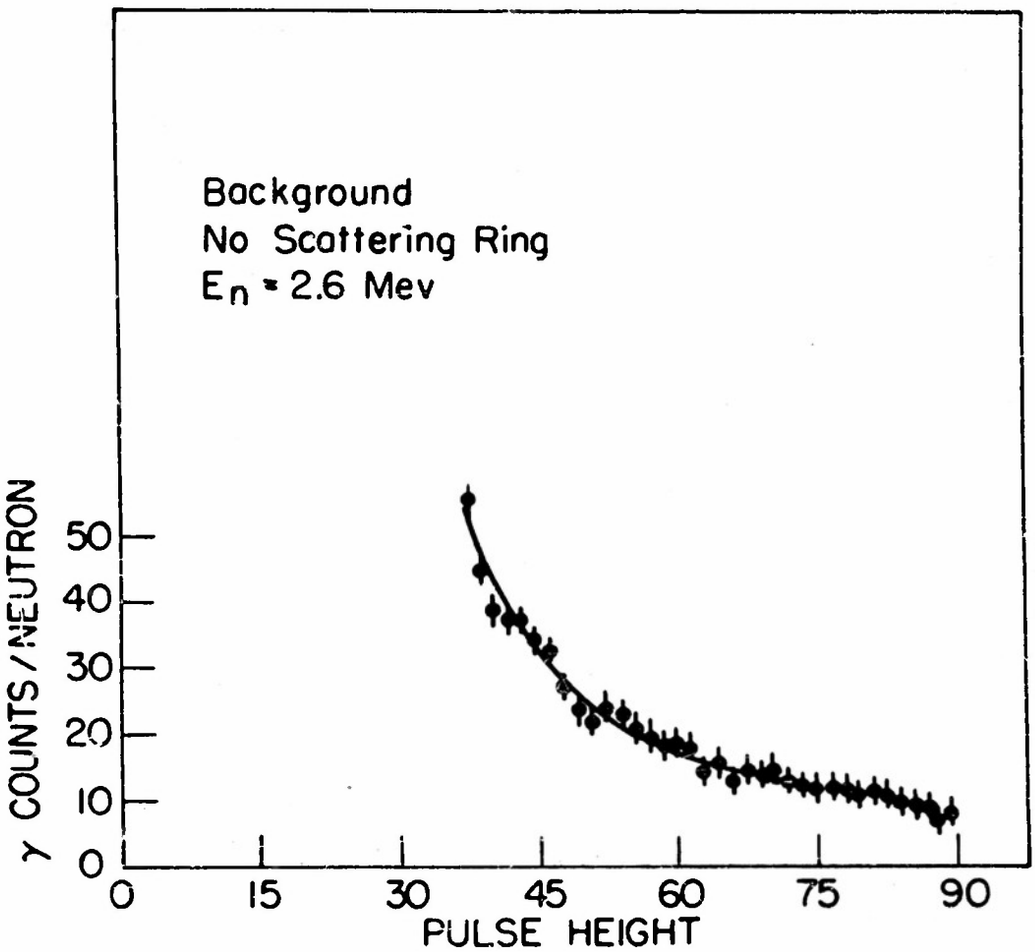

Fig. 18 Sample Gamma Ray Spectrum; No Scatterer. The single crystal NaI(Tl) spectrometer pulse height analysis gives an indication of the relative yield of the line spectrum of gamma rays superposed upon the continuous background. $\bar{E}_n$ = 2.6 Mev. In this case no scatterer was in position. The data give an indication of the effect of the cone in shielding the spectrometer. The background is observed to be a continuous spectrum.

escaping the scatterer in the direction $d\Omega$ of the crystal detector is proportional to

$$G = \beta \left\{ A \varphi_0 \frac{\Sigma_i}{\Sigma_t} (1 - e^{-\Sigma_t z}) \right\} \left\{ \frac{1 - e^{-n_a \mu T}}{n_a \mu T} \right\} \frac{d\Omega}{4\pi} \quad (2)$$

where n is the number of atoms per cubic centimeter, and $_a\mu$ is the total gamma ray absorption coefficient of the scatterer. Spherical symmetry of the resultant gamma radiation is assumed.

Of these gamma rays, the fraction

$$\frac{\tau}{\mu}(NaI) \left[1 - e^{-n\mu \bar{D}(NaI)} \right] \quad (3)$$

are absorbed by first collision photoelectric encounters in the NaI crystal of average thickness $\bar{D}$. τ and μ are the photo-electric and the total gamma ray absorption coefficients respectively of NaI. The photo-electrons produced in the crystal have their energy redistributed by crystal de-excitation into a number of light photons which is directly proportional to the energy of the incident gamma ray. These light pulses are observed with a photo multiplier and converted

into electrical pulses. As the number of secondary electrons produced in the photo-multiplier is proportional to the number of photons incident upon the photosensitive surface, the resulting gaussian distribution[19] of spectrometer output pulses has a half width σ which is proportional to $\sqrt{E_\gamma}$. The resulting pulse distribution has an energy distribution:

$$\frac{dN}{dE} = \frac{G}{\sqrt{2\pi}\,\alpha} \frac{e^{-\frac{(E-E_\gamma)^2}{2\alpha^2 E_\gamma}}}{\sqrt{E_\gamma}} \qquad \text{No. of gamma rays/}_{\text{unit energy}}$$

which has a maximum at $E = E_0$.

$$\left.\frac{dN}{dE}\right|_{max} = \frac{G}{\sqrt{2\pi}\,\alpha} \cdot \frac{1}{\sqrt{E_\gamma}} \qquad (4)$$

The resulting voltage pulse distribution has a maximum

$$\left.\frac{dN}{dV}\right|_{max} = \frac{dN}{dE} \cdot \left.\frac{dE}{dV}\right|_{max} = \frac{G}{\sqrt{2\pi}\,\alpha} \cdot \frac{1}{\sqrt{E_\gamma}} \cdot \frac{dE}{dV} \qquad (5)$$

Noting that

$$\varphi_0 = \varphi_{110^\circ} \left\{ \gamma_{0^\circ} / \gamma_{110^\circ} \right\}$$

and $$\frac{dE}{dV} = \frac{E_\gamma}{V_p}$$ (evaluated at peak),

the pulse height distribution has a peak height above background equal to:

$$\left.\frac{dN}{dV}\right|_{max} = P.H. = Const. \left[\frac{\phi_{110^\circ} Y_0^\circ}{Y_{110^\circ}} \frac{\Sigma_i}{\Sigma_t}(1-e^{-\Sigma_t z})\right]\left[\frac{1-e^{-n_a \mu T}}{n_a \mu T}\right]\left[\frac{\gamma}{\mu}\frac{(1-e^{-n_a \mu D\sqrt{E_\gamma}})}{V_p}\right] \quad (6)$$

Hence the peak height of the resulting gamma ray distribution is proportional to the inelastic neutron cross section, assuming that the total cross-section is known.

$$\sigma_{in} = Const. \left[\frac{P.H.\ Y_{\alpha_0}^\circ}{Y_0^\circ\ \phi_{\alpha_0}^\circ}\ \frac{\sigma_t}{(1-e^{-\Sigma_t z})}\right]\left[\frac{n_a \mu T}{1-e^{-n_a \mu T}}\right]\left[\frac{V_p}{\sqrt{E_\gamma}(\gamma/\mu)(1-e^{-n_a \mu D})}\right] \quad (7)$$

The first term in brackets is a function of the neutron energy, while the last two terms are functions of the gamma ray energy. An experimental verification of the last term in Eq. (7) was made by using Mn^{54} as a source of gamma rays and varying the position of the photo peak electronically, Fig. 19.

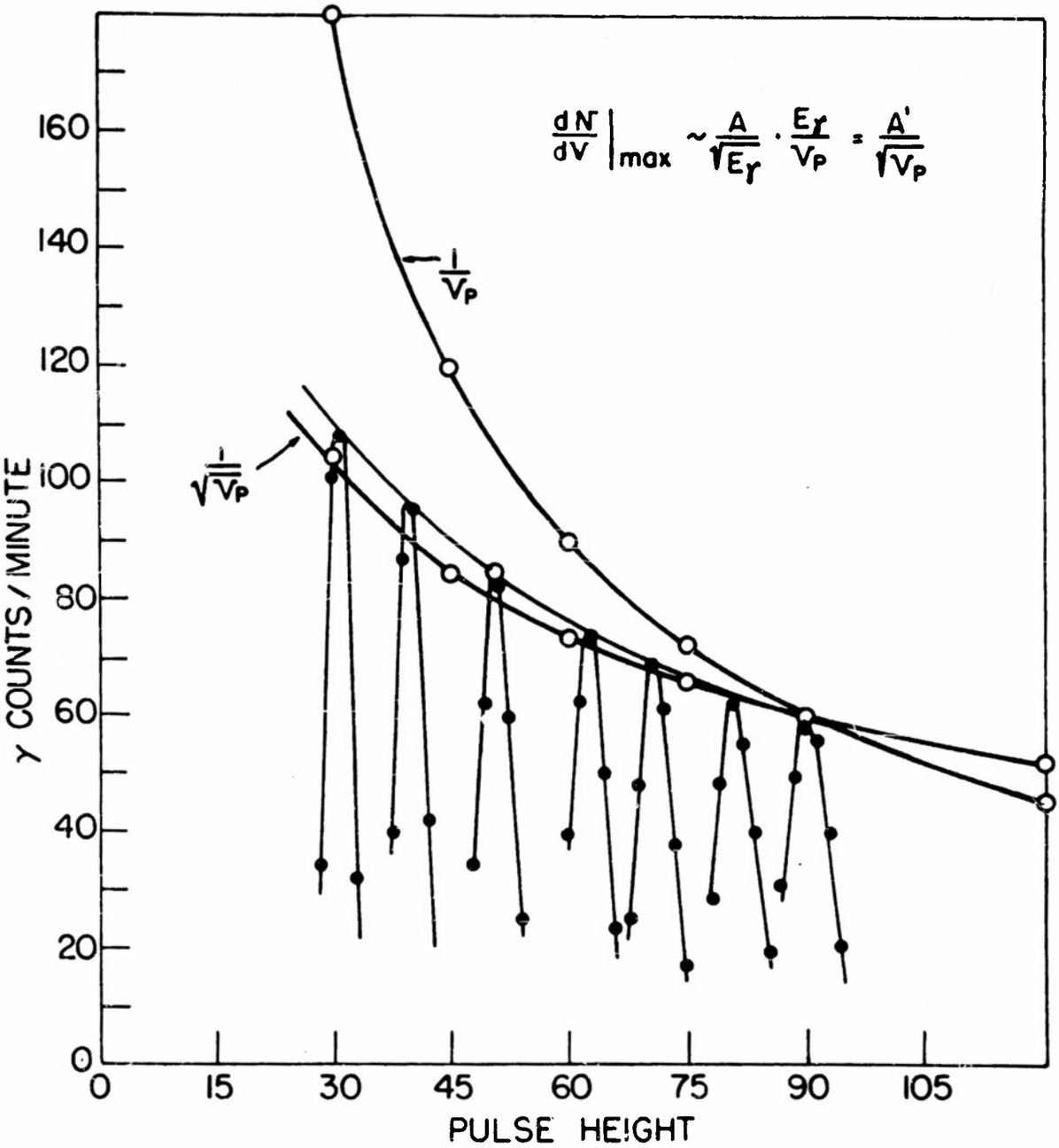

Fig. 19 Crystal Efficiency Factors. Eq. (6) of the text was experimentally checked by electronically positioning the photo peak from the Mn^{54} radiation at different voltage positions of the ten channel analyzer. Eq. (6) reduces to $\frac{dN}{dV}\Big|_{max} \simeq \frac{A}{\sqrt{V_P}}$ for a given gamma ray energy.

Once an absolute value for σ_{in} has been determined for one element, the preceding formula can be used to calibrate, to the first order, σ_{in}, for another element. Such corrections were used to obtain absolute values of σ_{in} for the other element studied herein, relative to Fe.

III-2 Calibrations

The calibrations of the equipment fall into three categories: calibrations of the neutron energy and energy width; calibration of the gamma ray energies and assignment of energy values for the excited states of the target nucleii; and the absolute calibration of the neutron inelastic scattering cross-section.

The neutron energy was determined by precisely measuring the incident proton energy to better than one part in 1000 and calculating the resultant neutron energy using the known Q values for the reactions used to produce the neutrons. Corrections were made for the target thickness by subtracting one-half of the target thickness in kev from the calculated energy. Further corrections were made for the energy spread resulting

from the angular dependence and the finite thickness of the conical scatterer. The target thicknesses, as determined by the geometrical peak of the neutron yield at the reaction threshold, varied between 15 and 25 kev. Total cross section resonances gave further checks upon the neutron energy determination.

The energy calibration of the gamma ray spectrometer was made by utilizing sources of known gamma ray energy: Co^{60} (1.33 Mev and 1.17 Mev), Cs^{137} (.661 Mev), Mn^{54} (.835 Mev) and Na^{22} (.511 Mev).[10] It was determined that the energy calibration of the spectrometer and the associated electronics equipment was linear to better than 3%. The resolution of the spectrometer and the geometry used was about 7.5% for the uncollimated .835 Mev Mn^{54} radiation. Better resolution was obtained with collimated gamma rays; i.e., 6.5% for the Cs^{137} (.661 Mev) radiation, Fig. 20.

When the energy values of the inelastically produced gamma rays were determined, the standard gamma ray sources straddled the unknown gamma line. The energy values given for the gamma rays observed are those determined by the spectrometer method; in some cases more accurate determinations have been made, which fall within

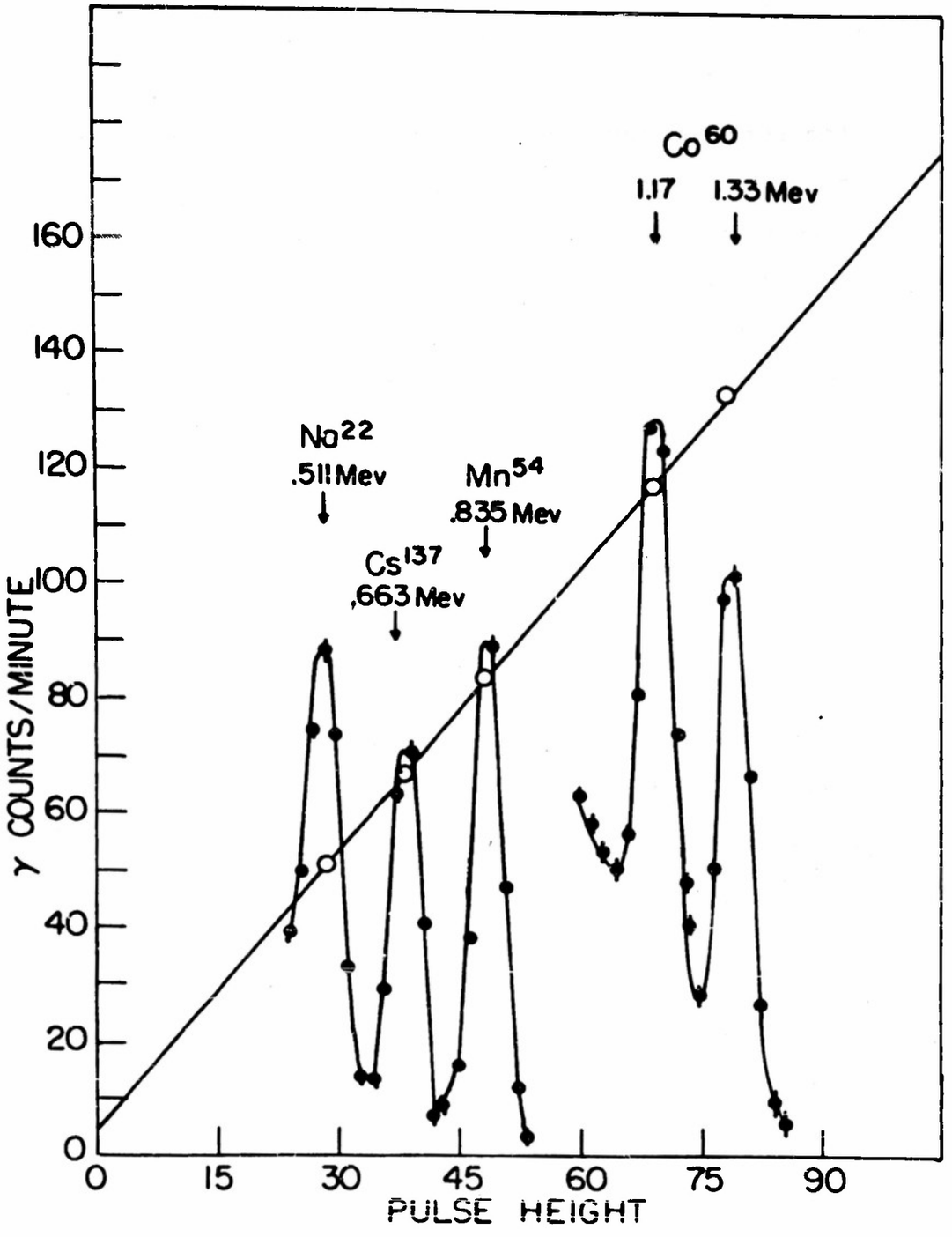

Fig. 20 Spectrometer Energy Calibration. The linearity and energy calibration of the single crystal NaI(Tl) Spectrometer was experimentally checked using known energy gamma rays: Co^{60}, Mn^{54}, Cs^{137}, and Na^{22}.

the spectrometer limits of error. The spectrometer error was taken to be one channel width, or about 2 → 3% in gamma ray energy.

The absolute values of the inelastic scattering cross sections were determined by utilizing Eq. (6). For a given gamma ray energy, Eq. (6) reduces to the product of two terms:

$$\text{P.H.} = \left.\frac{dN}{dV}\right|_{max} = (\text{Source Strength})(\text{Geometrical efficiency}) \quad (8)$$

For the case of an inelastically scattered neutron-produced source of gamma rays, the source strength is given by Eq. (1). Assuming the value of the neutron yield and Σ_T are known, all the quantities in Eq. (1) can be experimentally determined except Σ_{in}.

If one replaces the neutron produced source of gamma rays by a known radioactive source of approximately the same gamma energy, the geometrical efficiency may be determined experimentally. Coupling this result with Eqs. (1) and (8) yields an absolute value for σ_{in}.

Such a technique was used to determine the absolute inelastic scattering cross section for the 850 kev level in Fe^{56}. A known amount of Mn^{54} (E_γ = 835 kev)

was evenly evaporated on Fe shot, which was then loaded into a conical container. An experimental pulse height analysis was then determined, giving a value for the geometrical efficiency of the spectrometer-scatterer arrangement. A similar cone of non-radioactive Fe shot was put into position and bombarded by a computed number of neutrons. The pulse height data so obtained were analyzed using Eq. (8). An absolute value for the inelastic cross section in terms of the total neutron cross section resulted: $\sigma_{in}(Fe) = .59$ barn $\pm$ 10% at $E_n = 1.3$ Mev.

Another method of determing the absolute value of the neutron cross section σ_{in}, which depends only on a previous knowledge of the neutron capture cross section, was attempted but abandoned because of the low yield of neutrons available from the thin targets used in these experiments. Further work along the following lines should prove fruitful.

An element, such as Al, which produces a radioactive isotope emitting a known gamma ray and having a known capture cross section, is irradiated with a known flux of lower energy neutrons. The resultant pulse height distribution of the gamma ray emitted by the

radioactive isotope produced by the (n,γ) process is then measured, and the total number of radioactive atoms produced is easily computed.

$$\text{P.H.}\Big|^{(1)}_{\text{saturation}} = \text{const.}\gamma_a.\left(\frac{\text{No. of neutrons}}{\text{sec}}\right).\sigma_c.(\text{Geometrical efficiency}) \qquad (2)$$

The sample is then bombarded with the same number of high energy neutrons, and the resultant yield of inelastically produced gamma rays is determined.

$$\text{P.H.}^{(2)} = \text{Const.t.}\left(\frac{\text{No. neutrons}}{\text{sec}}\right).\sigma_{in}.(\text{Geometrical efficiency}) \qquad (2)$$

The geometrical efficiency may either be experimentally determined by the previous methods, or may be calculated from Eq. (7). Then,

$$\sigma_{in} = \frac{\sigma_c.(\text{P.H.})^{(2)}}{(\text{P.H.})^{(1)}_{\text{sat}}} \qquad \frac{G_{eff}^{(1)}}{G_{eff}^{(2)}} \cdot \frac{t}{\gamma_a} \qquad (9)$$

Once an absolute determination of σ_{in} for one elements has been made, Eq. (7) may be utilized to determine the value of σ_{in} for other elements, to the first order. Such a method was applied to Pb, Bi, Al, Ni and Cr, using the experimentally determined absolute value of $\sigma_{in}(Fe)$.

III-3 Measurements and Corrections

For each element studied an initial survey of the entire gamma ray spectrum emitted by the scatterer (from $.10 < E_\gamma < 3$ Mev) was conducted for several widely spaced incident neutron energies. Such investigations indicated the major inelastic gamma rays to be studied, Figs. 12 to 18. These gamma rays were further examined to see if they were due to cascade processes or decay to the ground state; i.e., an energy level scheme was developed for the target nucleus in question.

After the gamma ray lines were determined, the peak position was adjusted electronically to fit in the center of the entrance window of the ten channel pulse height analyzer and give simultaneously 10 data points over the

peak gamma distribution. The neutron energy was then increased in 25 kev to 100 kev steps, and the variation of the peak of the gamma ray line spectrum was recorded as a function of the neutron energy.

The photo-electric peak produced by the line gamma rays incident upon the NaI crystal is superposed upon the continuous spectrum of background gamma rays coming from (n,γ) processes in the NaI crystal, the scatterer and the room. A background correction can be determined by bombarding the scatterer with neutrons of energy slightly less than the energy of the excited level under observation. Such a spectral curve gives the shape of the necessary background correction to the line spectrum. The magnitude of the correction is adjusted to fit the background level, at each neutron energy, on the high energy side of the line spectrum peak, Fig. 21.

As Day had shown previously[2], the high resolution of the NaI single crystal spectrometer enables the separation of the line spectrum of gamma rays from the continuous spectrum of capture and background radiation, and from neighboring line spectra. The higher energy gamma ray (line spectrum) may always be measured effectively, but lower energy gamma rays may be obscured.

Fig. 21 Sample Gamma Spectra. The first curve on the left was taken with Li neutrons of 617 kev energy; the crystal was shielded with Pb. The gamma at 135 kev is attributed to the electric excitation of the Ta backing of the target. The other two gamma rays are attributed to $(n,n'\gamma)$ reactions in NaI. Note that there is no indication of a low lying level in Pb^{206}. The second curve, in two parts, is a typical spectrum of $Fe(n,n'\gamma)Fe$ taken below the first excited level in Fe^{56} at 850 kev (E_n = 820 kev; $T(p,n)He^3$), and above the first level (E_n = 1.01 Mev). The third curve of Co^{60} serves as an energy calibration, and gives an indication of the spectrometer resolution.

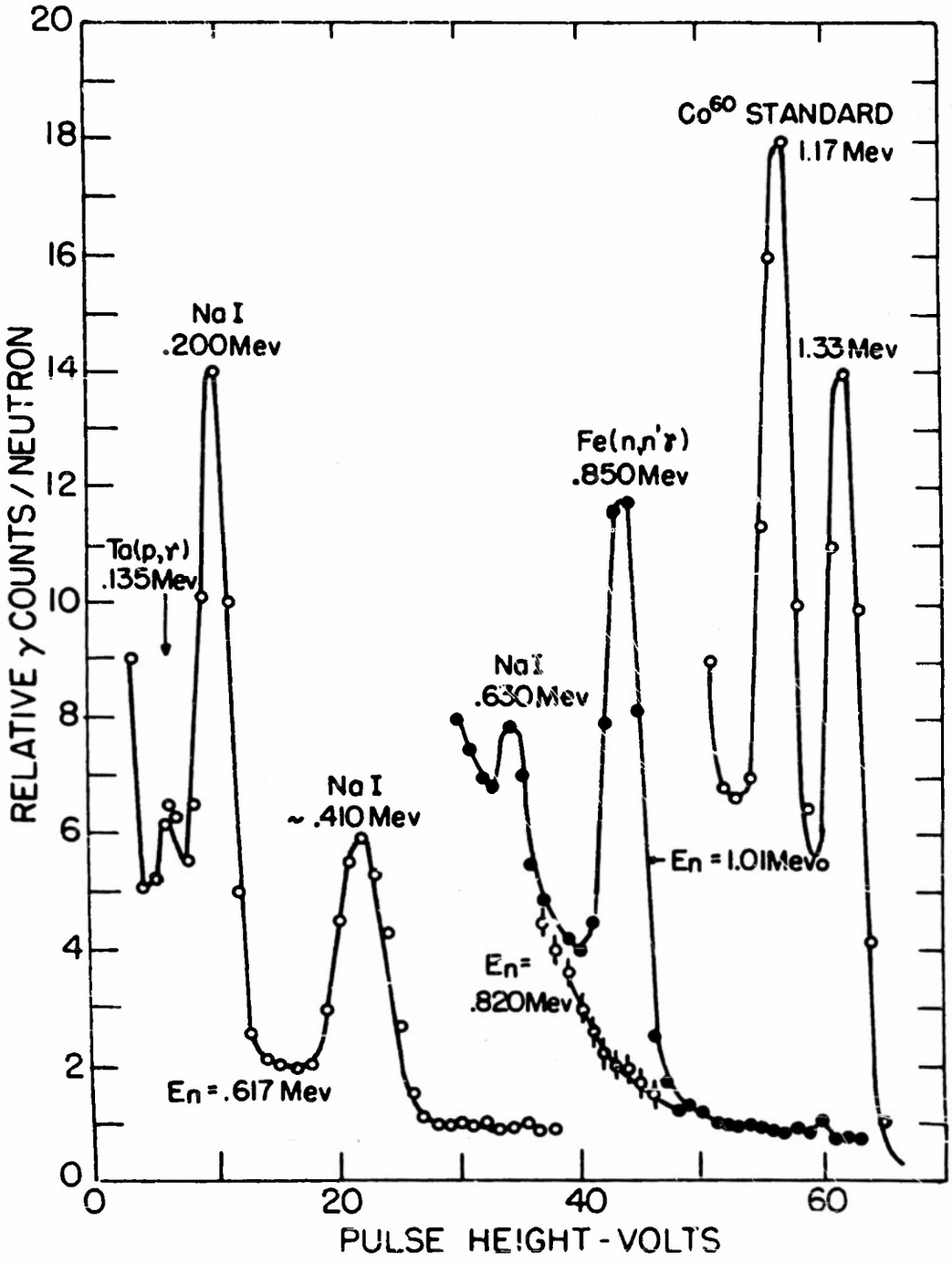
RELATIVE γ COUNTS / NEUTRON
PULSE HEIGHT - VOLTS
Co60 STANDARD
1.17 Mev
1.33 Mev
NaI
.200Mev
Ta(p,γ)
.135Mev
NaI
~ .410 Mev
En = .617 Mev
Fe(n,n'γ)
.850Mev
NaI
.630Mev
En = 1.01Mev
En=
.820Mev

When two or more levels are excited and emit gamma rays, the detection of the individual gamma yields becomes more complicated. The Compton distribution of gamma rays of higher energy will tend to add to the background which is to be subtracted from the lower energy photo-peak, decreasing the accuracy of the subtraction method. Moreover, if two gamma rays are close enough together in energy, the limited resolution of the spectrometer (~8%) may not allow the gamma rays to be distinguished. Such problems will be encountered when dealing with elements having a large number of isotopes or high level density ($A \gtrsim 150$). Nickel, which emits two gamma rays at 1.47 Mev and 1.33 Mev serves as an example, Fig. 15. The 1.47 Mev gamma ray distorts the spectral distribution of the 1.33 Mev gamma, and the low energy separation of the two photo peaks makes the determination of the true peak height of the 1.33 Mev gamma difficult. Obviously, the overall technique is then limited to the study of the inelastic scattering excitation of the first few levels of the target nucleus.

Further difficulties are encountered in single crystal spectrometry because the NaI crystal emits line gamma rays when subjected to neutron bombardment.

These gamma rays are due to neutron inelastic processes in the NaI crystal itself; the levels excited are at 200, ~410 and 630 kev, Fig. 21. As the scattering sample has an appreciable elastic scattering cross-section, a large fraction of neutrons incident upon the scatterer will be scattered into the NaI crystal producing (n,γ) and $(n,n'\gamma)$ reactions. The presence of the inelastically produced line spectrum of gamma rays in the crystal makes measurements of the inelastic neutron cross section of other elements, whose excited states produce gamma rays in the energy regions 150 to 250, 350 to 450 and 575 to 675 kev, extremely difficult to interpret. In the present work, only gamma rays of energy greater than 800 kev were studied successfully. It should also be noted that the gamma rays produced by neutron excitation of I^{127} are in partial cascade, which further complicates investigations in the above energy regions.

An eight inch cone of Pb was used to shield the crystal from the direct beam of neutrons and from gamma rays produced in the neutron source. Preliminary experiments proved that the cone was thick enough to self-absorb most of the inelastically produced gamma rays created within the Pb, Fig. 18. Experiments also

indicated that the cone was quite effective in protecting the crystal from the direct neutron beam, but neutron scattering from the conical ring under observation could be appreciable, Fig. 21.

Correction factors for the energy dependence of the efficiency of the crystal spectrometer were made according to Eq. (7), utilizing the experimental values of the gamma ray absorption coefficients for NaI[20], Fig. 22. The geometrical values used in Eq. (7) were:

*Z = 3.61 cm, T = 2.18 cm, and D = 4.71 cm.

The tritium target thickness was determined by the geometrical yield rise at threshold, E_p = 1.019 Mev; Fig. 23. The target thickness at other proton energies was determined from the theoretical specific ionization formula[29].

*For hollow cone used in calibration but not for solid scattering cones.

Fig. 22 Atomic Gamma Ray Absorption Coefficients for NaI. The atomic gamma ray absorption coefficients were calculated for NaI using the experimentally determined values for Na and I(ref. 20). The factor τ/μ plays an important part in the crystal efficiency terms used to intercalibrate the absolute values of the neutron inelastic scattering cross sections.

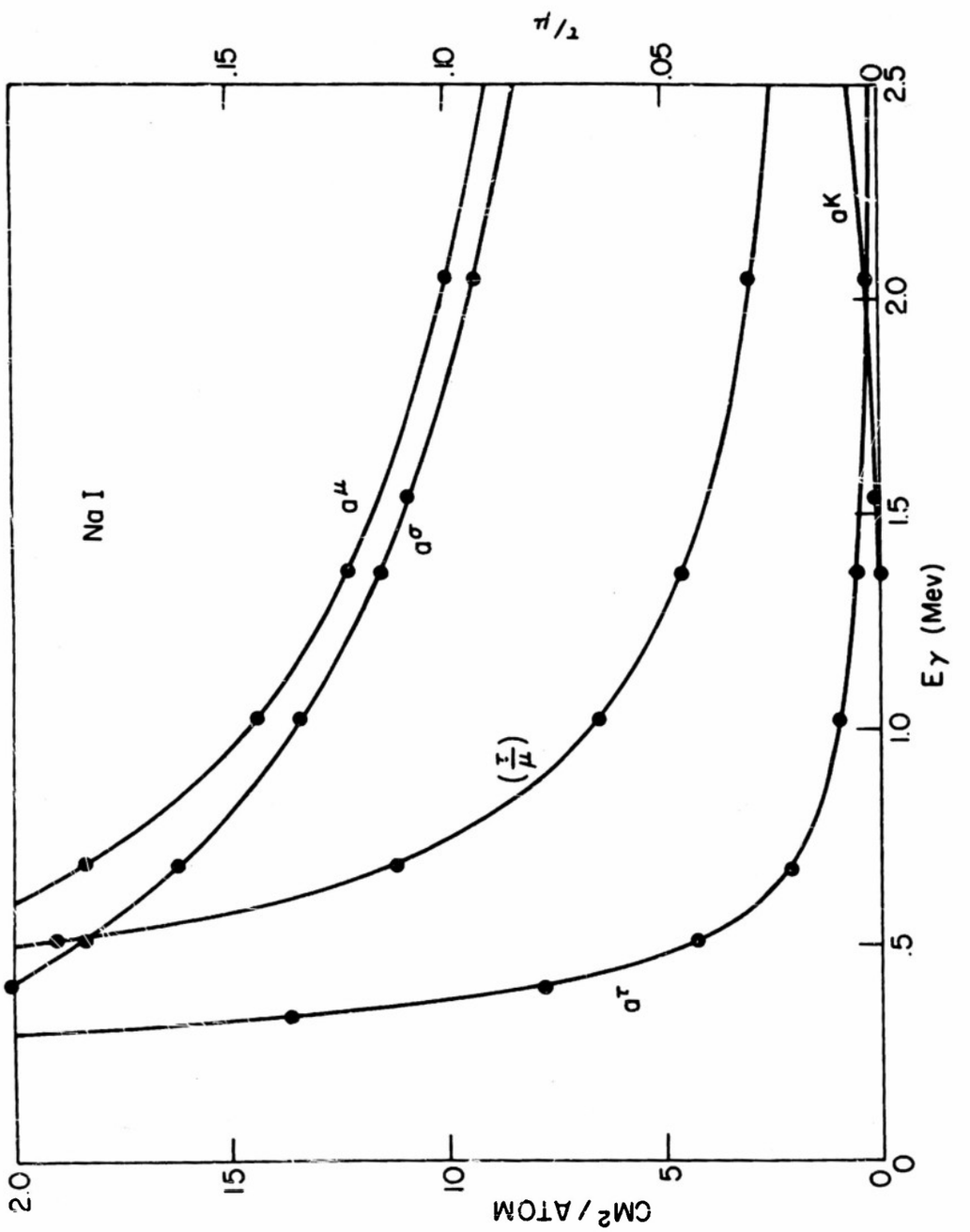
Na I
σ^{μ}
σ^{ρ}
$(\frac{\tau}{\mu})$
σ^{r}
σ^{K}
τ/μ
.15
.10
.05
0
2.5
2.0
1.5
1.0
.5
0
Eγ (Mev)
CM² / ATOM
2.0
15
10
5
0

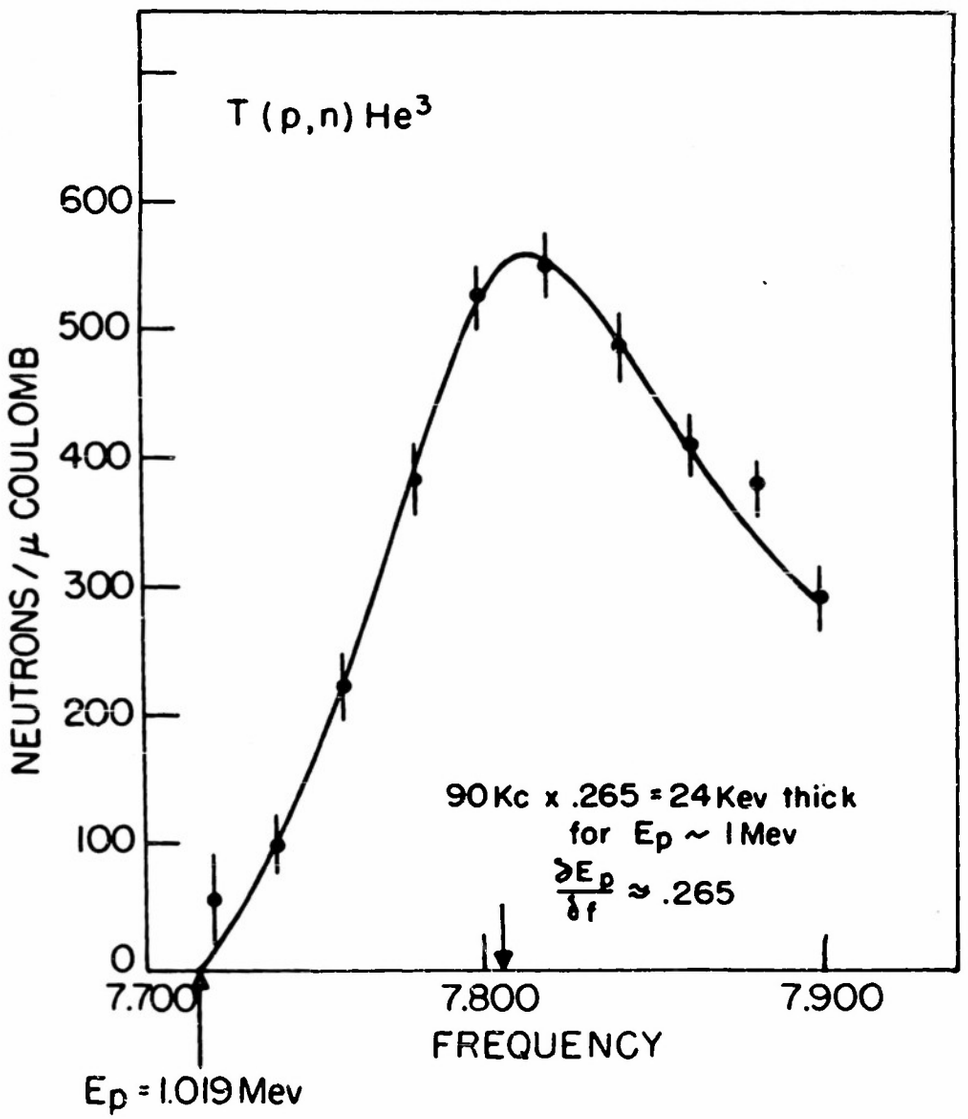

Fig. 23 Tritium Target Thickness. The tritium target thickness was determined by measuring in good geometry the peak position of the yield curve geometrical rise just above reaction threshold. The target thickness is equal to the proton energy difference between the peak and the threshold.

IV FUTURE EXPERIMENTS AND RECOMMENDATIONS

Besides the extension of the preceding techniques to more of the elements in the periodic table, a number of experiments utilizing similar methods suggest themselves.

Experiments should be conducted to determine the validity of the spectrometer efficiency factors, Eq. (7). Also, different energy gamma sources should be used for absolute calibrations of the inelastic neutron cross section as described in the calibration section. Capture activation methods of calibrating the absolute value of σ_{in} should be investigated more thoroughly.

In the preceding work corrections for beam attenuation were made on the basis of total cross-section averages because the total cross section had not been measured as accurately (energy-wise) as had the inelastic cross section, Fig. 11. For light elements, the total cross section should be known at least as accurately as the inelastic cross-section, in order that correlations of compound state resonances may be made accurately.

Coincidence techniques, utilizing two spectrometers, should yield information concerning cascade processes

and branching ratios of the excited states of the target nuclei. The yield of gamma rays and the efficiency of the crystal spectrometers so observed indicate that such experiments may prove to be possible.

Angular distribution of the inelastically scattered neutrons should be observable by making measurements of the gamma yield along the symmetry axis of the ring scatterer. In the preceding work the anisotropy of the gamma radiation has been neglected in the calculations of the cross sections. Experiments to determine if this assumption is valid should be conducted.

The effects of the poor geometry used in these experiments will have a tendency to give results which are averages over large angles, and the effects of a possible gamma ray anisotropy may be eliminated. The effects of multiple scattering and diffraction scattering in the sample could be investigated by a series of experiments giving the yield of gamma rays as a function of scatterer thickness.

Qualitative investigations have indicated that anisotropic corrections would have an effect of less than 15% on the results presented here.

Further attention should be given to the neutron inelastic scattering of the low lying rotational states in the heavy nuclei (Ta, W, Hf, etc.). These states, predetermined from a proton-Coulomb field interaction experiment[21], should inelastically scatter neutrons. It would be of theoretical interest to see if neutron excitation by surface waves could be observed. Those elements with large quadrupole moments should have the highest inelastic scattering cross sections for this process[23].

Although the statistical, compound nucleus theory seems to fit the Fe data quite well, it would be of even more interest theoretically to determine the inelastic cross-section for resonant processes. If gamma ray measurements could be made on some light element where the compound state level density is low, and the spins of the excited, ground, and compound states were known, interesting interpretations should result. As previously mentioned, B^{11} is a suitable element for such study. The first excited state has a spin $J = 1/2$ and is known to emit a gamma ray of 2.13 Mev. Compound states are excited at $E_n = 2.45$ Mev ($J = 2$, $\Gamma = 120$ kev) and $E_n = 2.58$ Mev ($J = 3$, $\Gamma = 60$ kev)[22]. A detailed study

of the 2.13 Mev gamma yield over the neutron energy range of 2.1 Mev to 2.8 Mev would yield information concerning resonance inelastic scattering. Silicon is another element which may be utilized, if the spins of the compound states can be determined from the total cross section data.

APPENDIX A

The Neutron Source; The Rockefeller Electrostatic Generator.

A mono-energetic source of neutrons was obtained by using the Rockefeller Electrostatic Generator[18] and the $Li^7(p,n)Be^7$ and the $T(p,n)He^3$ reactions[13]. Considerable effort was expended to put the Rockefeller machine back into operation and to raise the terminal voltage from 2.4 Mev at the beginning of these experiments to 4.3 Mev at the end. Proton currents averaging 5 microamperes would give relatively intense neutron yields for thin Li^7 targets (~25 kev thick). However, as the threshold value in the laboratory system of coordinates for the reaction $Li^7(p,n)Be^7$ is 1.882 Mev, a large fraction of the proton's energy was used up before neutrons could be produced. This handicap led to the acquiring of T impregnated in Zr targets, which would still retain the low neutron dispersion. Such targets were constructed, but due to the stopping power of Zr for protons, much lower yields of neutrons (by a factor of >100) necessitated an overall improvement in the

experimental method. The lower Q value for the tritium reaction was felt to be worth the trouble.

To test the reliability and the handicaps encountered in using the Rockefeller Generator in conjunction with the $Li(p,n)Be^7$ reaction as a controllable source of neutrons, a high resolution preliminary experiment was conducted involving the measurement of the total cross sections of Cl and P. (See Appendix C).

To increase the terminal voltage of the generator an equipotential shell was inserted at the one-third gradient point. To enable the corona load control system to function correctly, a moveable inner corona point was installed. Without the inner corona rod, the beam regulator would only function to control the voltage of the equipotential shell; the terminal voltage would be dynamically unstable for operation over the complete range of machine voltage. By proper adjustment of the inner corona rod position, the quiescent load on the regulating mechanism could be devised to appear as if the equipotential shell were not in place. Accordingly, for small dynamic variations, proper adjustment would decrease the dynamic time constant of the inner one-third voltage gradient such that proper control of the terminal voltage

could be obtained. (See Appendix B). The use of the equipotential shell lowered the voltage gradient on the upper part of the accelerating column, reducing stray corona and enabling the machine to operate up to 3.1 Mev.

A second improvement upon the pre-accelerating electrode of the beam focusing system enabled the machine to operate up to 4.3 Mev. Originally part of the focus voltage (-50 Kv) was obtained by the charging current IR drop through the focus power supply. Variations of charging current, or small column discharges, would tend to defocus the ion beam, allow it to spray along the accelerating tube walls and discharge the machine. Tests proved that the focus voltage needed to spot-focus the ion beam was approximately a linear function of the terminal voltage for the beam currents used in this machine. Accordingly the focus power supply was isolated from the charging current, and the entrance electrode to the column was placed always negative with respect to the focus supply by a suitable current loading resistor. Improved stability of the ion beam was immediately noticed. However, satisfactory operation was not obtained until an isolation shield was

established between the belt and the -50 Kv supply, cables, and focus electrode. Corona between the -50 Kv cable and the highly positively charged belt would initiate column breakdowns. High voltage x-ray cable insulation proved to be ineffective for this work, for once a breakdown occured, a corona weak spot always remained. A solid piece of Cu tubing, using the high pressure gas (which would regenerate its insulation properties) as an insulator, was finally installed as a focus cable. Immediately overall generator operation was improved and terminal voltage increased to 4.3 Mev, with a proton beam.

APPENDIX B

Corona Loading of Van de Graaff Accelerators.

One method of stabilizing and regulating the terminal voltage of Van de Graaff accelerators is to regulate the amount of corona leakage current between the high voltage terminal and the grounded pressure tank. Before a suitable controller may be designed, a functional description must be made of the process to be controlled. It is the purpose of this appendix to demonstrate that a servo-mechanism block diagram may be devised for the corona stabilization scheme, and that by standard servo-mechanisms analysis a suitable regulator may be devised to reduce ion beam wobble, and to increase analyzed beam output.

Essentially, a Van de Graaff accelerator is a large, parallel RC network supplied by a current source. The machine will charge up to a steady state potential, Vo, determined by the RC network of the generator and the net current supplied to the terminal, Fig. B-1. The net current is equal to the spray current supplied to the charging belt minus the corona leakage current, the beam current and the miscellaneous leakage currents. A

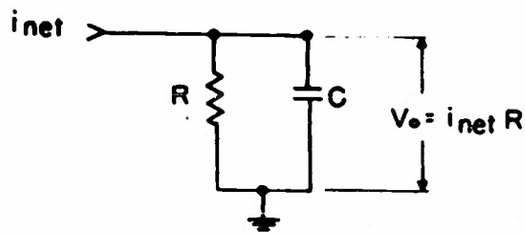

A. PASSIVE ELEMENT EQUIVALENT OF A VAN DE GRAAFF GENERATOR.

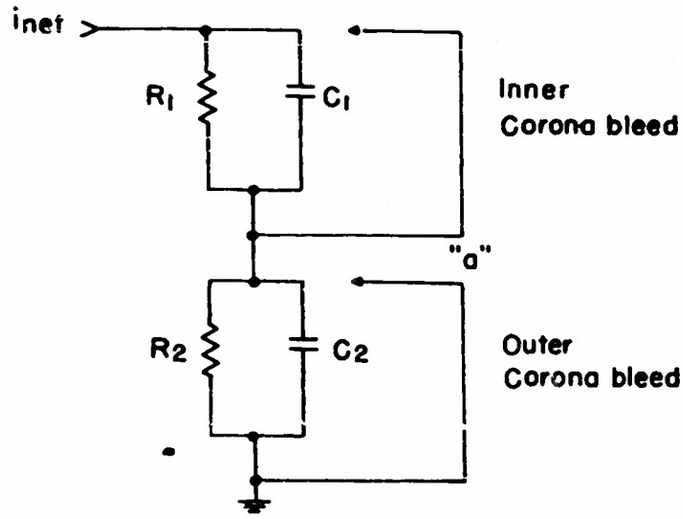

B. EQUIVALENT CIRCUIT FOR VAN DE GRAAFF INCLUDING EQUIPOTENTIAL SHELL

Fig. B-1 Equivalent Circuits for Van de Graaff Generators. A. No equipotential shell.
B. With equipotential shell.

beam of ions is accelerated down an evacuated column into a magnetic analyzer. Passing out of the analyzer the beam is defined by a pair of narrow slits. For a given magnetic field strength, only those ions which have been accelerated through a fixed potential difference will pass through the exit slits without hitting them. If the voltage is too low the beam will be deflected too much and will strike the upper slit; the collected charge may then be drained to ground through a resistor, and the resulting signal may be electronically amplified. Similarly, if the terminal voltage is too high, a signal can be obtained from the lower slit. Generally the slit system signals are fed to a difference amplifier, which then supplies the command signal to a controller which will regulate the amount of corona current which is allowed to leak away from the terminal through the gas to the tank walls.

The Corona Controller is generally a beam power tetrode connected in series with a corona rod through the tank wall. The tetrode control grid voltage is supplied by the difference amplifier.

The variation of the terminal voltage (variation of current supplied to the terminal) is compensated for

by a change in the corona load current. A functional diagram of the generator controller system is shown in Fig. B-2.

The analysis of the controller system is greatly simplified if one realizes that the generator in conjunction with the corona rod and pressure shell acts like a grounded grid triode. The plate of this triode is the high voltage terminal; the grounded grid is the high pressure shell; and the cathode is the corona rod.

Following the preceding assumptions, the circuit diagram for the generator may be drawn as in Fig. B-3. For incremental changes, the vacuum tubes are represented by the equation:

$$i_b = \frac{e_b}{r_p} + g_m e_c$$

Applying ordinary circuit analysis to Fig. B-3, and using the preceding equation, one obtains the result

$$\left\{1 + K\right\} \; i_c = \frac{V_o}{r_c} + g_T K \; V_B$$

where

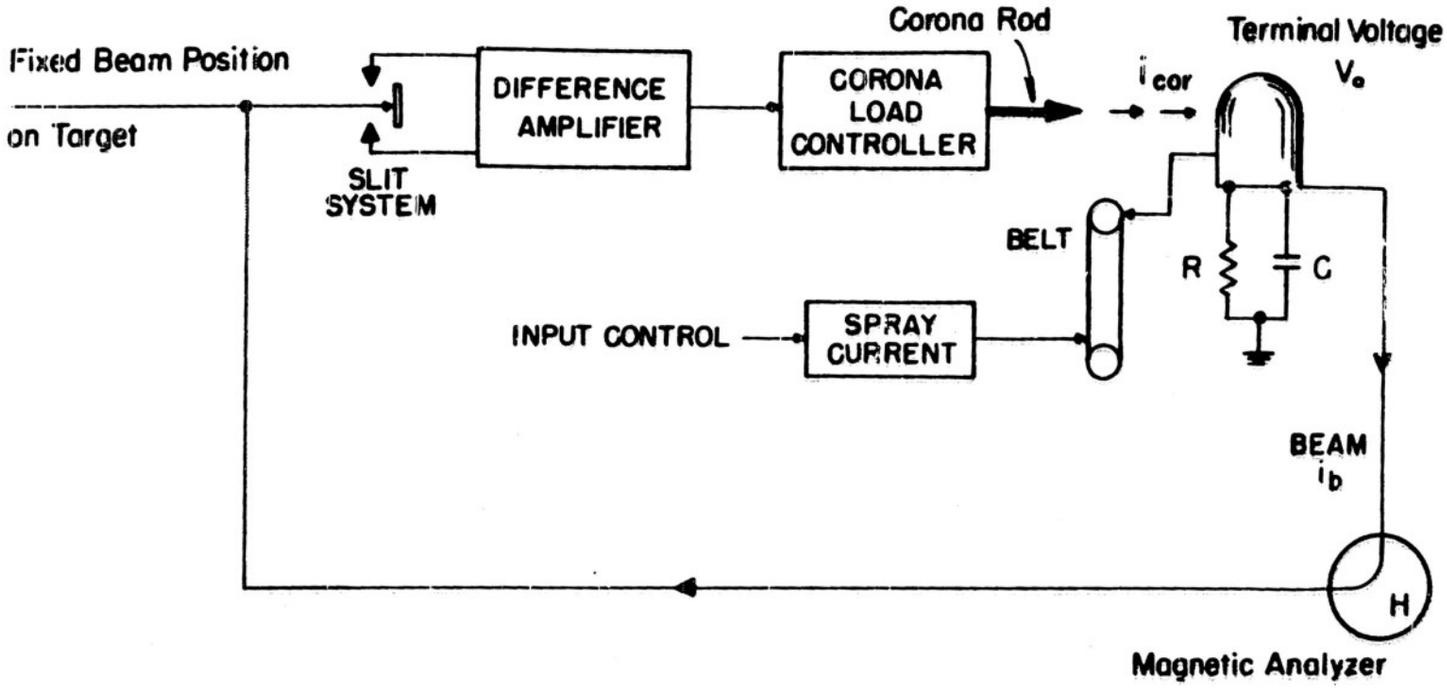

Fig. B-2 Functional Block Diagram of a Corona Controlled Van de Graaff Accelerator.

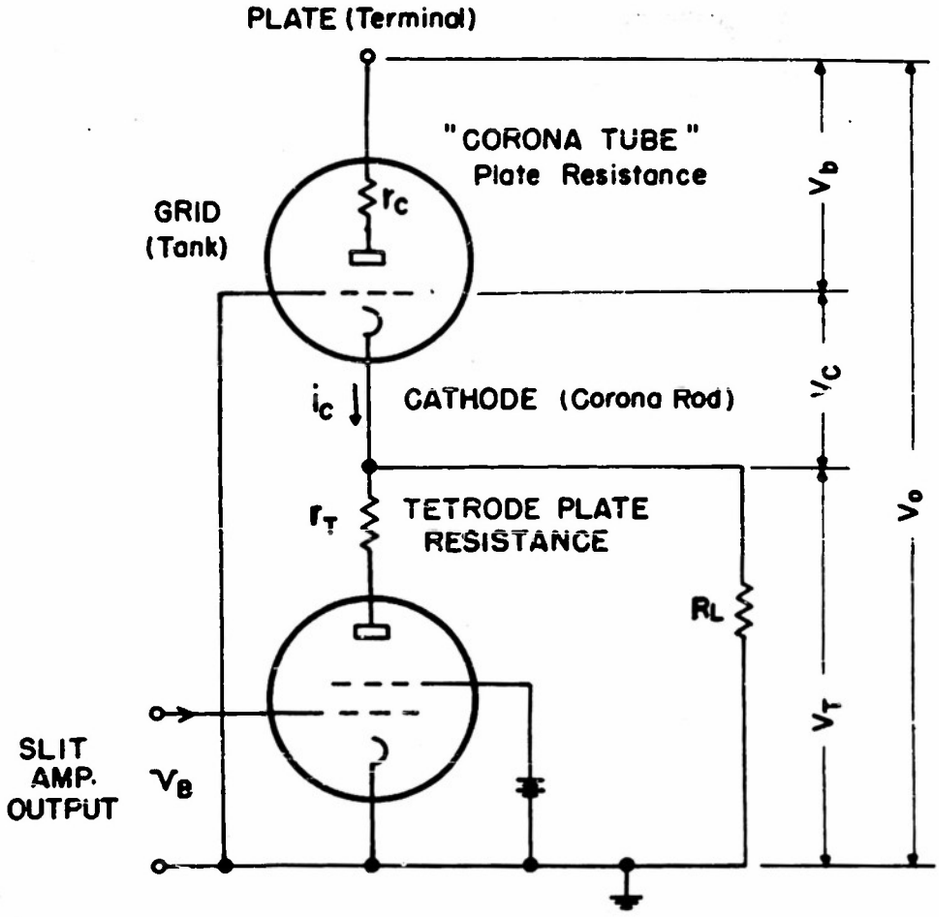

Fig. B-3 Tube Analogy for Corona Loading of Van de Graaff Accelerators. The Van de Graaff Generator is assumed to behave like a large, grounded-grid, vacuum-tube triode.

$$K = \frac{\frac{1}{r_c} + g_c}{1/r_T + 1/R_L}$$

and i_c = Corona current

V_o = Terminal voltage

V_B = Tetrode control grid voltage

r_c = "tube" resistance of the generator

g_c = transconductance of the generator

g_T = transconductance of the tetrode

r_T = tube resistance of the tetrode

R_L = load resistance of the tetrode

A similar linearization analysis will show that for small increments about a quiescent condition, the position error, $\Delta\chi$, of the beam is related to the variation of terminal voltage by the equation

$$\Delta\chi \sim \frac{Ro}{2Vo}\,\Delta Vo$$

Ro = Radius of analyzer

Vo = Terminal Voltage

for a 90° magnetic analyzer.

The Kirchoff equation at the current node of the terminal reads

$$i_s - i_{corona} - i_{misc} - i_{beam} = I_{net}$$

The block diagram for a parallel RC circuit fed by a constant current source is:

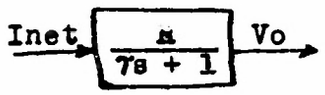

where RC = time constant of generator = τ

and

$$s = \left(\frac{d}{dt}\right)_{\text{operator}}$$

For a given beam current and for small deflections, Δx, the voltage induced on the grid resistor of the slit amplifier is

$$\Delta e \sim \frac{\Delta x}{\alpha} \frac{i_b}{R_g}$$

where α is the "effective" width of the beam at the exit slits. This voltage will be amplified by a factor K_1, the gain of the slit difference amplifier. The gain K_1 is the most easily adjusted parameter in the system, and should be designed for the best response. Faulty settings of K_1 will make the system oscillate and reduce analyzed beam output.

Hence for the linearized system, assuming operation only for small increments about quiescent values, an overall block diagram may be constructed as in Fig. B-4. The appearance of stabilizing feedback loops is immediately apparent.

To examine the amount of regulation offered by such a control system, one examines the beam position error, $\Delta\chi$, as a function of spray current variations (current losses). Ideally, for all frequencies $w > 0$, the ratio $\frac{\Delta\chi(w)}{i_s(w)}$ should vanish for perfect regulation.

Note that the regulator performance $\left.\frac{\Delta\chi}{i_s}\right|_{\chi_i = 0}$ can be interpreted in terms of the servo performance, $\left.\frac{\chi_o}{\chi_i}\right|_{i_s = 0}$ following standard servo-mechanisms analysis. It is important to remember that this is a regulator problem:

1) The beam position is the desired output quantity to maintain. The use of a magnetic analyzer insures that if the beam is to be positioned on the target, then the terminal voltage is determined by the analyzer and its geometry.

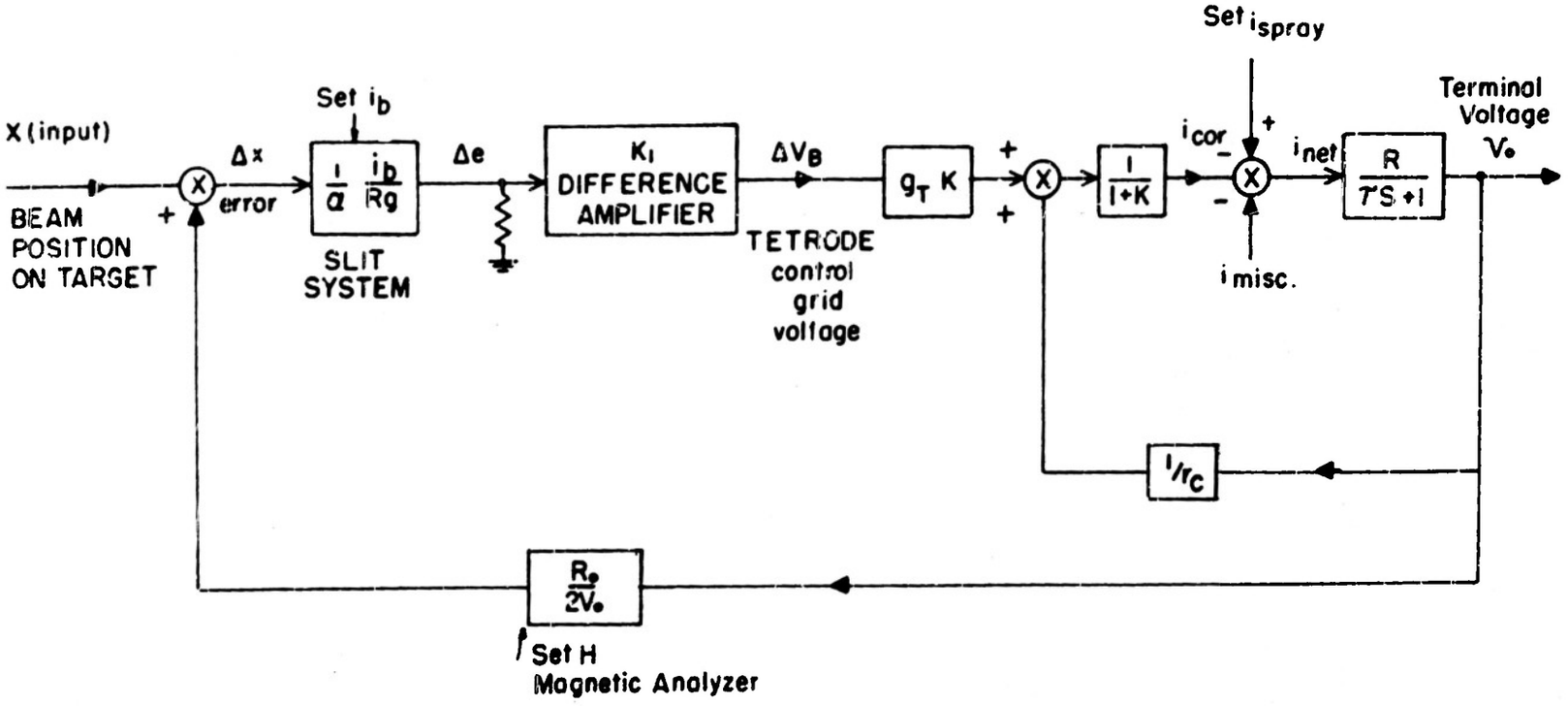

Fig. B-4 Servomechanism Block Diagram for a Corona Controlled Van de Graaff Accelerator. The appearance of the feedback stabilization loops is of particular interest.

2) The generator can be considered to be a parallel RC network with various current leakages. It is supplied from a current source (the belt and spray supply) i_s. Leakage currents are i_R - resistor stack; i_c - transient reactance current; i_{Cor} - corona discharge current; i_m - miscellaneous leakage currents from pulleys, skirt, inductor bar, etc.

3) The servo analysis comes under the general category of multiple disturbances in closed loop systems. Correct gain settings and corrective network designs can now be determined from the basic servo diagram using standard techniques. With the Rockefeller machine, the analogy made to a grounded grid triode has been checked experimentally.

For systems which have an intermediate equipotential shell, the analysis is slightly modified. The machine is now represented by two parallel RC networks in series, Fig. B-1. It may be shown that for suitable stabilization of the inner terminal voltage, a current path (corona) must be established between the inner terminal and the

equipotential shell; otherwise, the outer corona rod controller merely regulates the voltage of the equipotential shell, and the inner terminal is dynamically uncontrolled.

A moveable inner corona point will be effective in providing the additional "inner" corona current needed. Ideally, the inner corona current from the terminal to the equipotential shell should be adjusted to equal the outer corona current from the equipotential shell to the outer corona rod. Then, for small dynamic changes point "a" of Fig. B-1 is a current node, and may be removed from the diagram; i.e., the equipotential shell is then dynamically of no importance. The corona regulator produces its effects directly upon the inner terminal as desired.

In the Rockefeller machine it was found experimentally that unless some provision was made to change the inner corona current drain, the machine would not remain dynamically stable over its full range of voltage operation (.8 to 4.3 Mev).

APPENDIX C

The Crystal Spectrometer

To effectively separate the line spectrum of inelastic gamma rays from the high background of capture and scattered gamma rays, and in some cases from a neighboring line spectrum, considerable effort was expended in constructing high resolution NaI spectrometers[19].

Initially, polished crystals immersed in Nujol for tight optical coupling with RCA-5819 photo-multipliers were used. Resolutions of the order of 12% (resolution defined as peak width at half peak height divided by peak position in Mev) for the Cs gamma ray (E_γ = .661 Mev) were obtained after careful selection from thirty 5819 tubes. Careful polishing, good reflecting surfaces and tight optical coupling are necessary for high resolution work, but it was determined that even the most careful effort was inadequate if a poor photo-multiplier was used. Ideally the spectral response of the photo-multiplier tube should be matched to the spectral emmission of the NaI crystal, which peaks in the blue region.

Experiments were made with colored oils to determine qualitatively the importance of this effect. Blue and colorless oil gave the same resolution, but red and yellow oils greatly reduce the resolution. This effect is important with oil immersed crystals, for residual alcohol dissolves the NaI slightly and colors the oil yellow. Hence after a period of time, the resolution of the spectrometer decreases.

The commercial RCA 5819 tubes vary considerably from tube to tube, not only in spectral response, but, more importantly, in cathode sensitivity. For high resolution spectrometers photo-multipliers of greater than 40 micro-amperes/lumen cathode sensitivity are needed. The RCA 5819's tested averaged about half this value, with perhaps one tube in fifty exceeding it.

Harschaw dry-air packed, MgO coated NaI crystals were used with the DuMont 6292 photo-multipliers. The DuMont tubes have a minimum sensitivity of 40 micro-amperes/lumen and range as high as 70 micro-amperes/lumen. Close optical contact crystal and photo-multiplier is still required. A suitable technique is to wrap the crystal with a sheet of plastic forming a sealed tube which is filled with Nujol. The flat faced photo-multiplier

is then inserted within the plastic tube until it makes contact with the window at the end of the crystal container. The whole assembly is then wrapped with two layers of electrical insulation tape which both seals in the oil and acts as a light shield. When large crystals (1 1/2" x 2") are used the whole assembly is very easy to construct, very portable, and stable for many months. Using the above technique spectrometers were easily constructed which had a resolution of 7%, or better, for cesium gammas.

The photomultiplier and preamplifier were housed in a tubular aluminum case. The effect of stray magnetic fields was reduced by enclosing the photo-multiplier in a mu-metal shield. The photo-multiplier was also shielded from the adverse effects of gamma rays striking the dynode surfaces by a 3/8" thick tube of Pb.

APPENDIX D

Electronics.

The first electronics requirement for gamma spectrometry is a highly regulated, extremely well stabilized power supply. Due to the high amplification factor of the photomultiplier tube, extreme demands are made for power supply stability. If a resolution uncertainty as large as .5% due to power supply variation is tolerable, the power supply still must be stable to better than .05%.

Precision wire wound resistors, which have a low temperature coefficient should be used in the voltage dividing network for the photomultiplier dynodes and preamplifier, Fig. E-1. The amplifier should be a medium gain, fast rise time, voltage amplifier within which provision for delay line pulse shaping can be utilized.

It was necessary to develop and construct a ten channel pulse height analyzer in order to accumulate data rapidly and conveniently when thin Zr - T targets were used. The neutron yield and the inelastic gamma yield is so low that single channel analysis of the gamma ray pulse height spectrum is intolerably long. A 6BN6

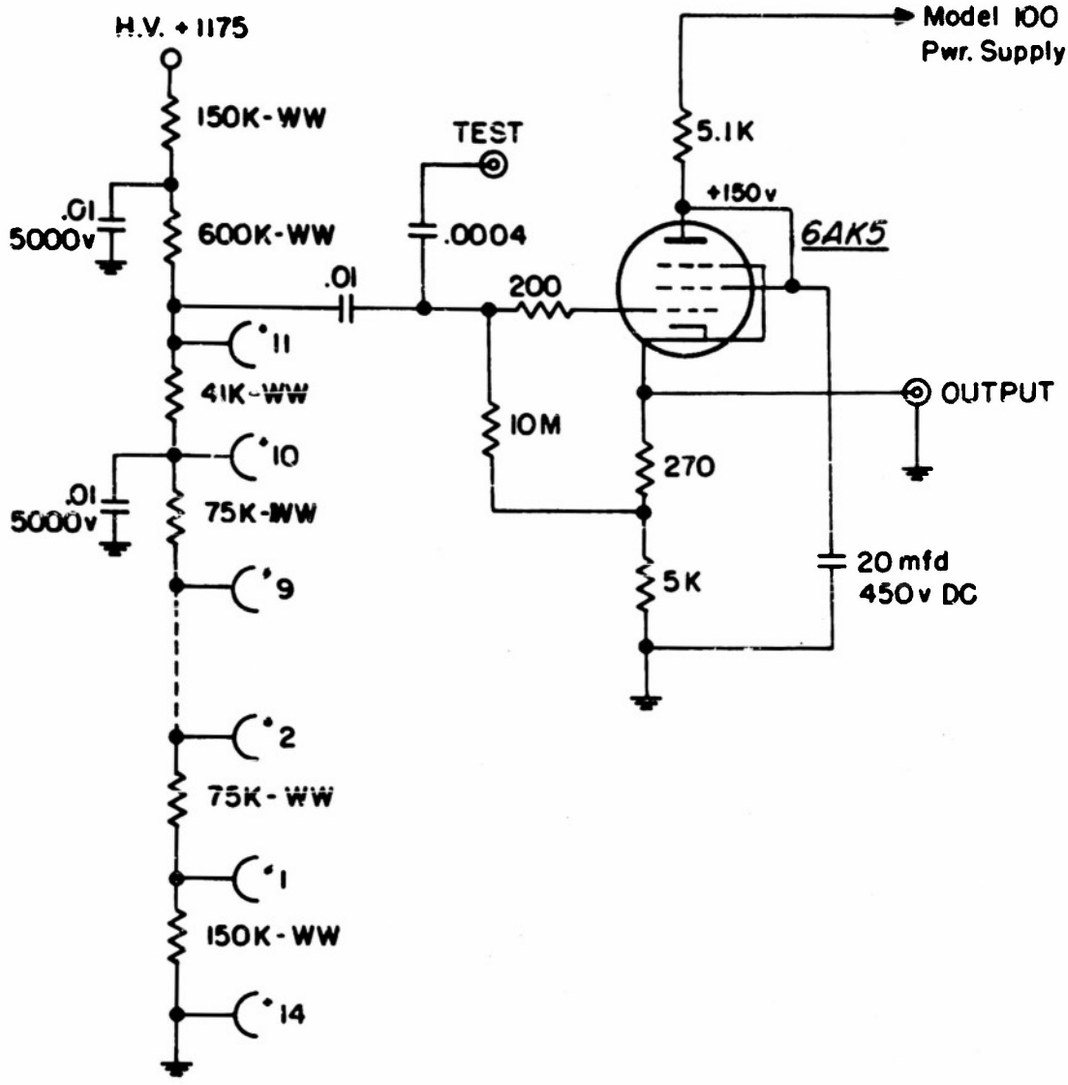

Fig. E-1 Photomultiplier Pre-Amp.

discriminator, R-C mixed anti-coincidence network, ten channel analyzer, similar to the Los Alamos design[25], was constructed, Fig. E-2. Remote control instrumentation and ten remote decade scaling units utilizing the new Philips tube were also designed and constructed, Fig. E-3.

An expander amplifier was designed (see Appendix F) to convert the ten channel analyzer into the equivalent of a 100 channel device, (1% window width at the output) Fig. E-5.

The overall stability of the analyzer has proven to be adequate for the experiments conducted. The precision is excellent, and the ease of operational adjustments underlies the simplicity of the design. Recalibration of window widths may be done to $\pm$2% in a period of one-half hour with the aid of a sliding pulser. These window widths remain stable within $\pm$3% over a two week period. Peak heights have been stable to 2% for the same period. All power supplies and detectors were powered by Sola regulating transformers. An overall electronics block diagram appears in Fig. E-4.

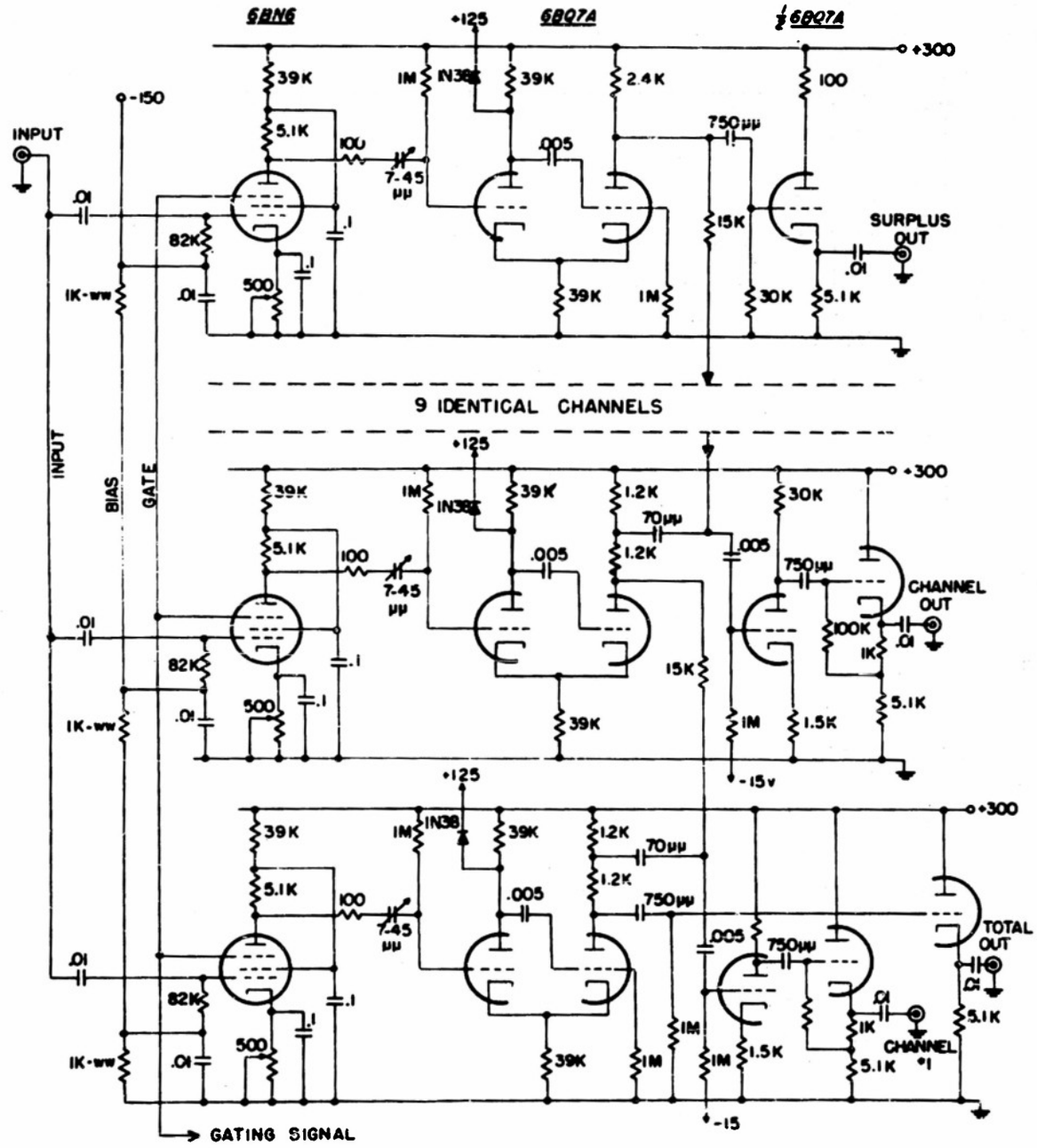

Fig. E-2 Model L.A.S. Pulse Sorter.

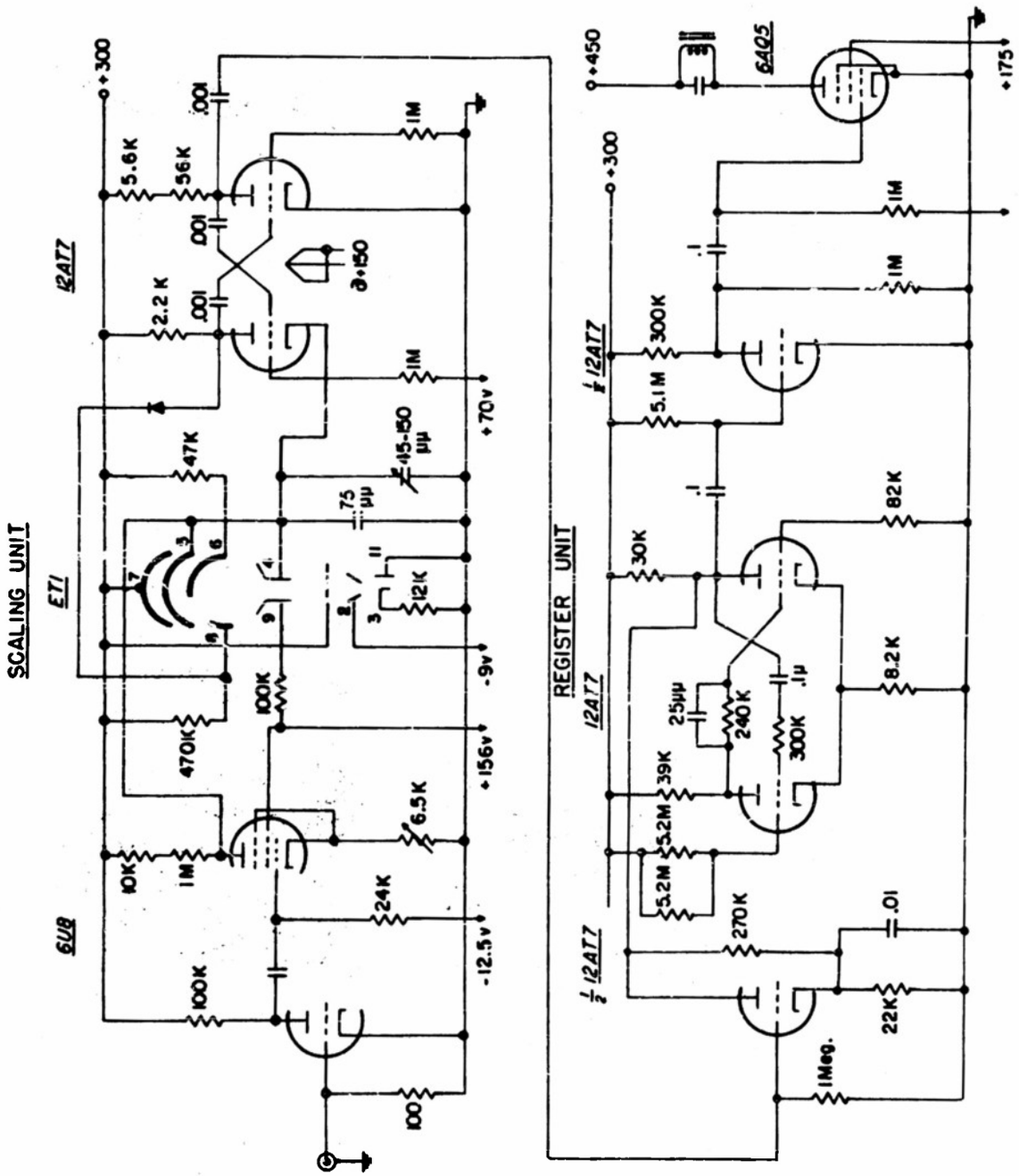

Fig. E-3 Model L.A.S. Decade Scalers.

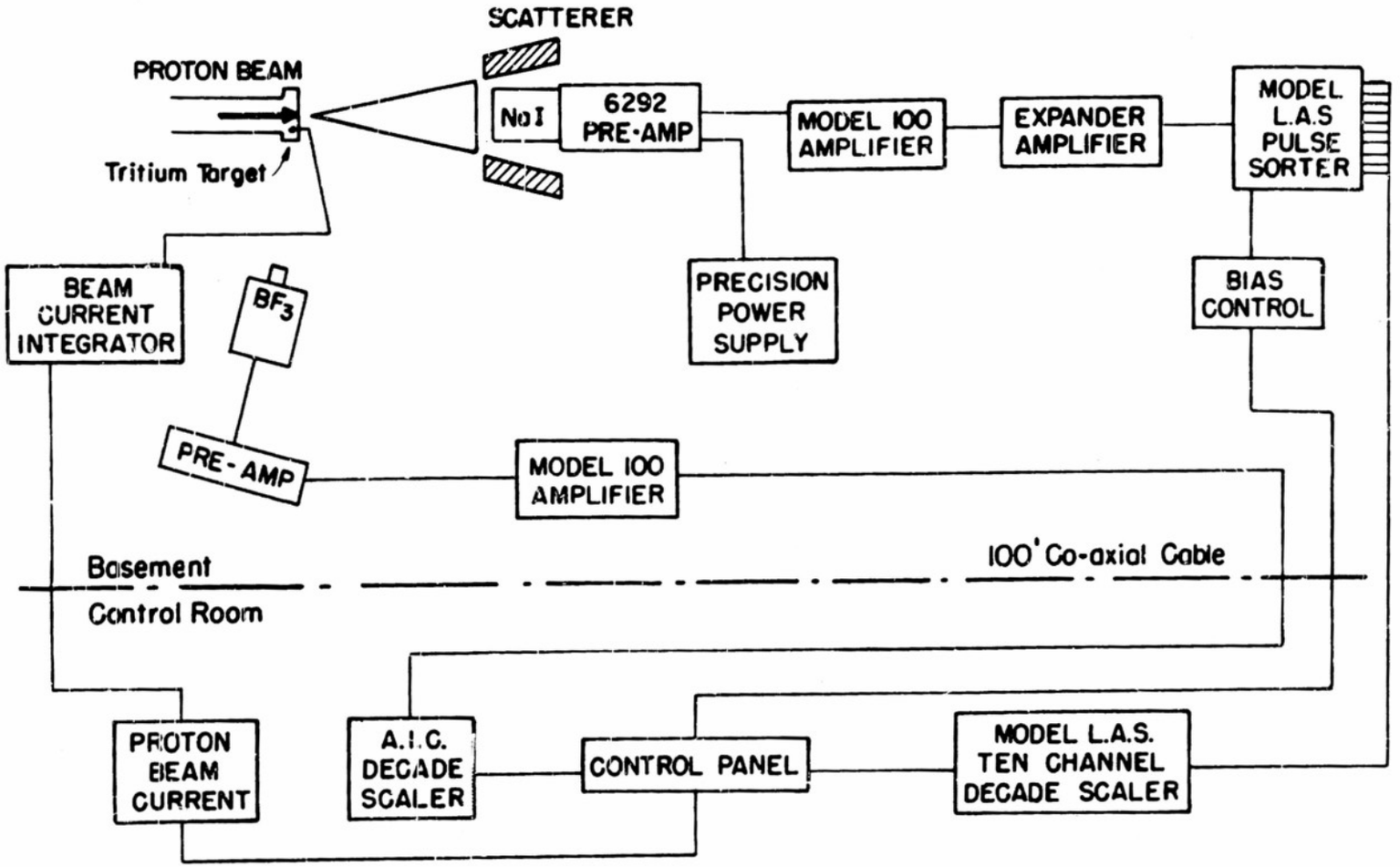

Fig. E-4 Overall Electronics Block Diagram.

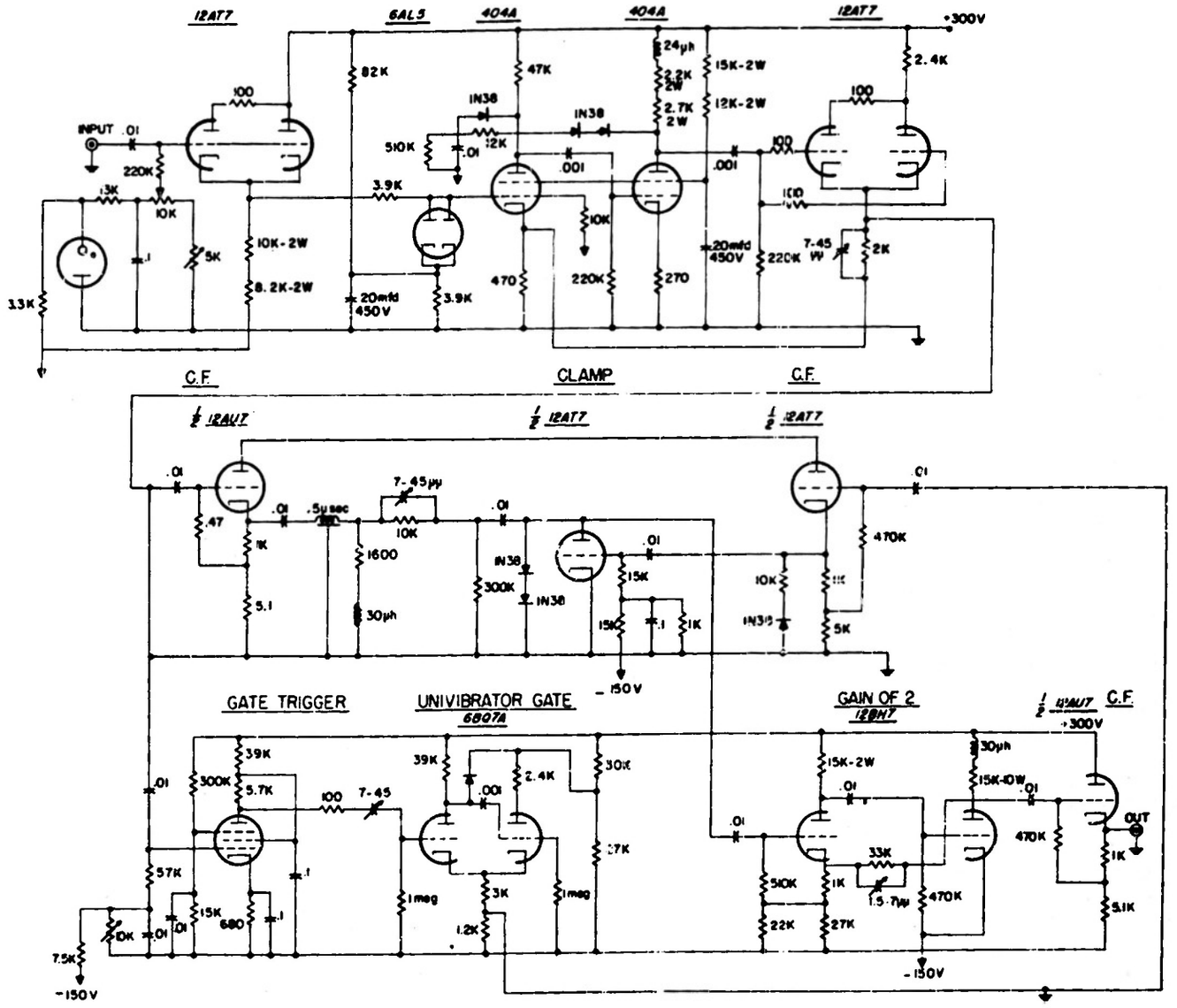

Fig. E-5 Expander Amplifier

APPENDIX E

An Improved Expander Amplifier for Gamma Ray Spectrometers.

A simple, effective method of reducing the duty cycle on the discriminator sections of a multi-channel pulse height analyzer has been developed. In high resolution gamma ray spectroscopy narrow window widths (1% of total voltage of 100^{V}) are required for accurate definition of a complex spectrum. Commonly, a ten channel analyzer, preceded by an expander amplifier, will have an entrance window of the order of 10% of the total voltage spectrum (i.e., 10^{V}). Pulses which fall below the entrance window are not transmitted; those which fall above are amplified by a factor of 10 and saturated as an overload pulse. One purpose of the expander amplifier[26] is to saturate these overload pulses "gracefully", i.e., without overshoot. However, it has been standard practice to admit to the discriminator all overload pulses, which must first trigger every discriminator channel and then lodge in the surplus channel. In practice the number of overload pulses may be larger than 100 times the number of pulses in the entrance window. Accordingly, the discriminators work 100 times harder than is necessary.

A simple, gated linear clamp network has been devised to stop the overload pulses from reaching the discriminator channels, Fig. F-1. A 6BN6 tube, triggered by the original pulse, is used in conjunction with a univibrator to produce the gating signal. The 6BN6 is biased to trigger for only those pulses which reach the full amplitude of the expander amplifier, i.e., the saturation pulses. A .5μ sec delay is used to insure that the clamp is either fully opened or closed by the time a pulse (1μ sec width) reaches it. The clamp is gated on the 3μ secs by the expander output signal. The expander output signal is attenuated by a factor of about 2/3 by the attenuated delay line. While the clamp is off the signal is further attenuated by a factor $\frac{5K}{300K + 5K} = 1.6\%$. The signal is then amplified to a maximum of 100^{V} by a gain of two feedback amplifier. When the clamp tube is on, the signal is attenuated by a factor of $\frac{5K}{5K + 300}$ 96% which produces a pedestal pulse of 8^{V} at the output for all saturated overload pulses produced by the expander. As the first bias level at the discriminator channels is 10^{V}, none of the expander overload pulses actuate the discriminators.

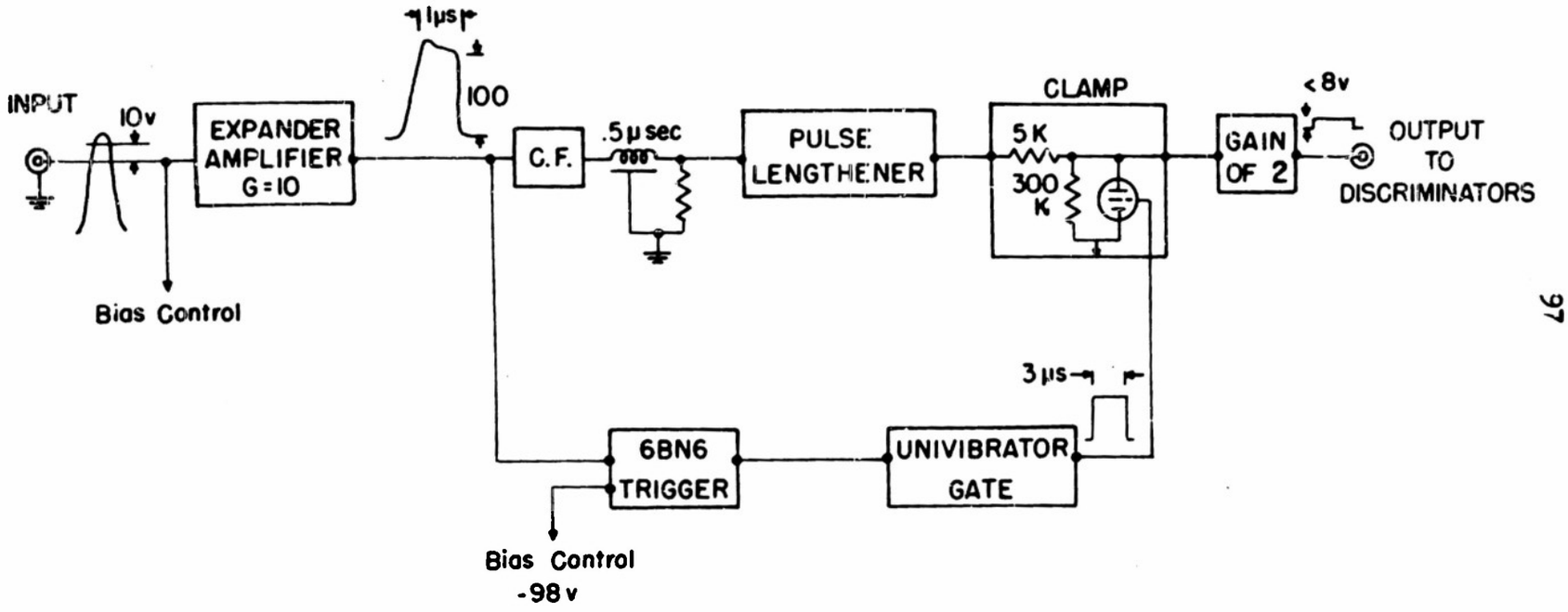

Fig. F-1 Expander Amplifier and Duty-Cycle-Limiter Block Diagram.

A pulse lengthener (optional) may also be included within the circuit to reduce the bandwidth specifications on the discriminator channels.

APPENDIX F

Targets

The reactions $Li^7(p,n)Be^7$ and $T(p,n)He^3$ were used as sources of neutrons in the energy interval 0 to 2.8 Mev[13]. Very thin lithium targets (2 to 5 kev) may be utilized for poor geometry experiments, because of the high yield of neutrons from the lithium reaction.

Thin (25 kev) tritium targets were made by diffusing T_2 into Zr with an estimated absorption of $ZrT_{1.1}$. However, the large stopping power of Zr prohibits the effective use of much thinner ZrT targets because of the low neutron yield from the low concentration of tritium. Proton beam currents of the order of 5μamperes are needed, with 25 kev thick ZrT targets, to obtain enough neutrons to permit the experiments to be conducted in a reasonable time.

The absence of a secondary group of neutrons, and the lower Q value of the $T(p,n)He^3$ reaction more than make up for the difficulty in producing thin tritium targets.

The ZrT targets were mounted on a tungsten backing which was air cooled to remove the 10 to 20 watts of heat generated by the proton beam.

APPENDIX G

The Neutron Monitors.

Enriched BF_3 "long" counters were used in addition to proton current to monitor the neutron flux incident upon the scatterer. The response of these long counters was assumed to be flat for neutrons from 200 kev to 2.8 Mev. Preliminary experiments were conducted in good geometry to obtain a calibration between the neutron flux incident upon the scattering sample and the neutron flux as detected by the neutron monitors at 90^{o} with respect to the proton beam for both the $Li^{7}(p,n)Be^{7}$ and the $T(p,n)He^{3}$ reactions.

Model 100 amplifiers and preamplifiers were used in conjunction with Atomic Instrument decade scalers. The high voltage on the counter was adjusted to obtain an optimum neutron to gamma sensitivity ratio.

APPENDIX H

Absolute Calibration.

In short the calibration was achieved by using a known amount of radioactive material to replace a neutron created source of gamma radiation of essentially the same energy.

A known source of γ rays from the radio-isotope Mn^{54}, was evenly distributed on a known weight of iron shot by evaporation of an aqueous solution of $MnCl_2$. The source strength was $3.34 \times 10^6 \gamma$/min.[27]. One-tenth of this solution gave an adequate experimental counting rate. Gamma-ray measurements of the container and evaporation dish indicated that less than five per cent of the radio-isotope remained in the containers; it was assumed that all of the isotope was distributed on the shot.

The radioactive iron shot was placed in a hollow truncated scattering cone, and a pulse height analysis was made to calibrate the scintillation counter, including the effects of solid angle, crystal efficiency and self absorption.

A similar cone of non-radioactive iron shot was then bombarded with high energy neutrons (~1.3 Mev). The number of neutrons incident on the scattering cone was determined by measuring the lithium target thickness - by means of the geometrical yield rise at threshold - and the proton current incident upon the sample. The Los Alamos data[13] were used to compute the yield of neutrons from the reaction $Li^7(p,n)Be^7$. The solid angle was determined by geometrical measurements.

The Mn^{54} radiation (E_γ = 835 kev) approximates very closely the gamma ray energy obtained by neutron excitation of the first excited state of Fe^{56}. The possible effects of anisotropy of the gamma radiation of the neutron produced source have been neglected, as the "poor" geometry used serves to average over the angular distribution.

For a given gamma ray energy, the pulse height maximum of the experimentally determined gamma ray spectrum equals

$$\left.\frac{dN}{dV}\right|_{max} = G.S$$

where G is the geometrical efficiency and S is the source strength.

Neglecting uncertainties in the Los Alamos data for the neutron yield from the reaction $Li^7(p,n)Be^7$, the inelastic scattering cross section of Fe was determined to be: $\sigma_{in} = .587$ barn $\pm$ 10% at $E_n \simeq 1.3$ Mev. The following calculations demonstrate the method, and give an indication of the source of errors.

Mn^{54} Radiation.

$S = .334 \times 10^6 \gamma/\text{min}(\pm 5\%)$

$\frac{dN}{dV}_{max} = 1780\gamma \text{ counts}/_{\text{min}}(\pm 3\%)$

therefore $G = \frac{1780}{.334 \times 10^6} (\pm 5.8\%)$

$Fe^{56}(n,n'\gamma)Fe^{56}$ Radiation: $E_n \simeq 1.3$ Mev

$S = \frac{\text{Neutrons}}{d\Omega} \cdot d\Omega \frac{\sigma_i}{\sigma_t} (1-e^{-\Sigma_t Z})$

where $\frac{\text{Neutrons}}{d\Omega} = (\text{Target thickness})(\text{proton current}) \frac{y_{\theta}^{\circ}}{\text{kev-}d\Omega\text{-}\mu C}$

target thickness = 65 kc x .36 = 23.5 kev($\pm$5%)

proton current = 8.58 μcoulomb $\pm$ (.5%)

Yield (Los Alamos) = $\frac{4.28 \times 10^6}{40}$ neutrons, s/dΩ-kev-μC

$$d\Omega = \frac{dA}{k^2} = \frac{T.2\pi\bar{R}}{(Ro/\cos\varphi)^2} = \frac{(.75)\pi(3)}{(8.6/.982)^2}$$

$$= .092 \text{ steradians } (\pm 2\%)$$

σ_t = 2.4 barns (Oak Ridge Data)($\pm$9%)

Z = 3.81 cm. (length of scattering cone)

Density of Fe shot = 685 grams/200 cm^3 = 4.43 gms/cc

$$\Sigma_t Z = (.0845)\left(\frac{4.43}{7.85}\right)(2.4)(3.81)$$

$$= .437 \ (\pm 10\%)$$

$$\frac{1 - e^{-\Sigma_t Z}}{\Sigma_t} = \frac{1 - e^{-.437}}{.116} = 3.08 \pm (4\%)$$

Hence

$$S = (23.5)(8.58)\left(\frac{4.28 \times 10^6}{40}\right)(.092)(3.08)\,\Sigma_1$$

$$= \sigma_{in} \ 2.93 \times 10^5 \quad (\pm 6.7\%)$$

$$\left.\frac{dN}{dV}\right|_{max} = 920(\pm 4\%) \ \gamma \text{ counts}$$

$$\text{therefore } \sigma_1 = \frac{\left.\frac{dN}{dV}\right|_{max}}{G.\ 2.93 \times 10^5} = \frac{920}{1780}\,\frac{3.34 \times 10^5}{2.93 \times 10^5}$$

$$= .587 \text{ barn } (\pm 10\%)$$

In order to compare the results of these experiments with the Los Alamos sphere experiments which used a fission spectrum of neutrons, it is necessary to formulate an effective group inelastic scattering cross section, defined by the equation:

$$\sigma_{in}(\text{group}) = \frac{\int_{E_1}^{E_2} \chi_F \sigma_{in}\, dE}{\int_{E_1}^{E_2} \chi_F\, dE}$$

where χ_F is the fission spectrum and was approximated by

$$\chi_F = .484\, e^{-E} \sinh \sqrt{2E}$$

for neutrons of energy E Mev. The Los Alamos results[15] for $0.4 \leq E \leq 1.4$ are:

Element	Los Alamos σ_{in}(group)	Integrated Experimental Data
Al	.07 ± (100%) barn	.085 barn
Fe	.313 ± .1	.33
Bi	.168 ± .1	.10
Pb	.168 ± .1	.04 (Pb^{206} only)
Au	.9	
Cd	.581	
V	.217	

The large uncertainty in the LA data make this comparison of limited value.

APPENDIX I

Theoretical Calculations.

Calculations based upon the Hauser-Feshbach[17] theory of inelastic scattering were computed for the following transitions, Figs. 2 to 8.

$0^+ \rightarrow 1^+$

$0^- \rightarrow 1^-$

$0^+ \rightarrow 2^+$

$0^+ \rightarrow 0^+$

$9/2^+ \rightarrow 7/2^+$

The values of T_ℓ were determined by graphical interpolation of curves appearing in the final report of the Fast Neutron Data Project[28]. Values for the nuclear radius were taken from total cross section data as given in Blatt and Weisskopf[14]. The calculations only considered those transmission coefficients for which $0 \leq \ell \leq 3$ and $0 \leq \ell' \leq 3$.

It should be remembered that the statistical assumptions made about the compound nucleus imply that all possible J compound states are available at all energies - certainly not a realistic approach. The

success of the theory is remarkable, when one considers that the statistical assumption for the compound nucleus is not true, and that the transmission coefficients were computed for the "black" nuclear model[14].

REFERENCES

1) Beghian *et al*, Phys. Rev. 82, 969L (1951)

2) R. B. Day, Phys. Rev. 89, 908 (1952)

3) B. Rose and J. M. Freeman, Proc. Phys. Soc. Lond. A66, 120 (1953)

4) P. H. Stelson and W. M. Preston, Phys. Rev. 86, 132L (1952)

5) B. G. Whitmore and G. E. Dennis, Phys. Rev. 84, 296 (1951)

6) P. H. Stelson and C. Goodman, Phys. Rev. 82, 69(130A) (1951)

7) D. D. Philips, R. W. Davis and E. R. Graves, Phys. Rev. 88, 600 (1952)

8) L. Szilard *et al*, Phys. Rev. 74, 1216A (1949)

9) B. T. Feld, Phys. Rev. 75, 1115 (1949)

10) U. S. Department of Commerce, "Nuclear Data", NBS 499 (1950)

11) H. M. Neumann and I. Perlman, Phys. Rev. 81, 958 (1951)

12) J. M. Hollander, I. Perlman and G. T. Seaborg, Rev. Mod. Phys. 25, 469 (1953)
G. Scharff and N. Goldhaber, Phys. Rev. 90, 587 (1953)

Hausman, Allen, Arthur, Bender and McDole, Phys. Rev. 88, 1296 (1952)

13) A. O. Hansen, R. F. Taschek and J. H. Williams, Rev. Mod. Phys. 21, 635 (1949)

14) J. M. Blatt and V. F. Weisskopf, "Theoretical Nuclear Physics", Wiley, N.Y., (1952)

15) R. D. Beister, Personal Communication

16) AECU-2040, "Neutron Total Cross Sections"

17) W. Hauser and H. Feshbach, Phys. Rev. 87, 366 (1952)

18) W. M. Preston and C. Goodman, Phys. Rev. 82, 316A (1951)

19) R. Hoftstadter and J. A. McIntyre, Nucleonics 7, 32 (1950)

20) C. M. Davidson and R. D. Evans, Rev. Mod. Phys. 24, 79 (1952)

21) C. L. McClelland and C. Goodman, Phys. Rev. 91, 760 (1953)

22) F. Ajzenberg and T. Lauritsen, Rev. Mod. Phys. 24, 321 (1952)

23) A. Bohr and B. R. Mottelson, Dan. Mat. Fys. Medd. 27, No. 16 (1953)

24) G. S. Brown and D. P. Campbell, "Principles of Servomechanisms", Wiley (1948)

25) C. W. Johnstone, Nucleonics 11, 36 (1953)

26) A. B. Van Rennes, Nucleonics 10, 22 (1952)

27) C. Borkowski, Personal Communication

28) AEC Report NYO 636

29) D. Halliday, "Introductory Nuclear Physics", Wiley N.Y. (1950)

30) B. Margolis, Phys. Rev. (in press) Dec. 1, 1953.

ACKNOWLEDGEMENTS

The author wishes to express his most sincere appreciation to the Gulf Oil Corporation for the financial support in the form of the Gulf Oil Fellowship, which made this graduate work possible.

Many members of the Neutron Physics group have given freely of their time in assisting with these measurements. Matti K. Salomaa was of particular help with the construction of the electronics equipment. Dr. T. H. Magel made the T-Zr target which was extensively used in these experiments. Dr. Caspar Borkowski, of the Oak Ridge National Laboratory, calibrated the Mn^{54} standard used for determining the absolute values of the inelastic scattering cross section.